Dissertation

Biocompatibility analysis of different resorbable Magnesium alloys in a rat model

Submitted by

Pt. Metapt. Anastasia MYRISSA

For the Academic Degree of

Doctor of Medical Science

at the

Medical University of Graz

Department of Orthopaedics and Orthopaedic Surgery

under the Supervision of

Assoz.-Prof. Priv.-Doz. Dr.med.univ. Annelie-Martina WEINBERG, MBA

Graz, 2016

Statutory Declaration

I hereby declare that this thesis is my own original work and that I have fully acknowledged by name all of those individuals and organisations that have contributed to the research for this thesis. Due acknowledgement has been made in the text to all other material used. Throughout this thesis and in all related publications I followed the "Standards of Good Scientific Practice and Ombuds Committee at the Medical University of Graz".

Date 23.08.2016 *Anastasia Myrissa*

Dedicated to

my parents and Stavros

Acknowledgments

It would have not been possible to complete my thesis without the support and help of a number of people.

First of all, I would like to thank my supervisor, Annelie-Martina Weinberg, for her continuous support and guidance. I am indebted to her for the chance she gave me to be part of her team and get involved in such a challenging project.

I was very lucky to meet and collaborate with some kind and supportive people, whom I consider not only as my colleagues but also as my friends and my family. Many thanks to Elisabeth Martinelli, Johannes Eichler and Claudia Kleinhans for their kind help, their precious advices and, most significantly, for the friendly and welcoming atmosphere which they created over these years.

Moreover, I would like to thank all the people in the MagnIM Project and in the BRIC Project. Special thanks to Regine Willumeit-Römer, for her support and to Peter Uggowitzer for his helpful advices. Through inspiring and helpful meetings and workshops, I was able to enrich my knowledge and improve my skills.

I would also like to thank Elmar Willbold, from Medizinische Hochschule Hannover, for his mentoring during my training in Hannover and for his time whenever I needed his help or advice and Ute Schäfer for her support.

This research work would not be possible without the funding from the People Programme (Marie Curie Actions) of the European Union's Seventh Framework Programme FP7 (2007-2013) under REA Grant Agreement No 289163.

Last but not least, I would like to thank my family and my partner, Stavros, for their constant and unconditional support as well as their invaluable help over these years.

Table of Contents

Abbreviations

alpha-MEM	Minimum Essential Medium
Ag	Silver
Al	Aluminium
Ca	Calcium
Ce	Cerium
DAB	Diaminobenzidine
DMEM	Dulbecco's Modified Eagle Medium
DR	Degradation Rate
Dy	Dysprosium
EDTA	Ethylenediaminetetraacetic acid
FBS	Fetal Bovine Serum
Gd	Gadolinium
HE	Hematoxylin-Eosin
HZG	Helmholtz-Zentrum Geesthacht
ICPQQQMS	inductively coupled plasma triple quadrupole mass spectrometry
La	Lanthanum
M	mean
MEA	2-methoxyethyl acetate

Mg	Magnesium
Mn	Manganese
Mg-Ag	Magnesium-Silver alloy
Mg-Gd	Magnesium-Gadolinium alloy
NAOH	Sodium Hydroxide
Nd	Neodymium
PBS	Phosphate-buffered saline
REE	Rare Earth Elements
SD	Standard deviation
TBS	Tris-buffered saline
TRAP	Tartrate Resistant Acid Phosphatase
T4	solution treatment
T6	ageing treatment
WZ21	Magnesium-Yttrium-Zinc alloy
ZX50	Magnesium-Zinc-Calcium alloy
Zn	Zinc
Zr	Zirconium
µCT	micro-focused Computer Tomography
3D	3-dimensional

List of Figures

List of Tables

Abstract in English

Introduction Biodegradable Magnesium (Mg) materials are under investigation because of their promising properties as orthopaedic devices. Different chemical elements like Rare Earth Elements (REE) are used as alloying elements in the Mg alloys to enhance the mechanical properties and the degradation resistance. Their possible usage in bone fractures, especially in children, raises many questions regarding their applicability and safety. In most of the studies, the degradation properties and the biocompatibility of Mg alloys are analyzed *in vivo* by using micro-focused Computer Tomography (μCT). However, histological analysis with Technovit 9100 New embedding method can provide further and more detailed information about how and whether the degradation performance can affect and interfere with the bone cells during the bone healing process.

Materials and Methods Distal epiphysis femoral bones were used to establish histological staining protocols for rat bones embedded in Technovit 9100 New. Cylindrical pins of pure Mg (99.99%) and two binary Mg alloys, Mg2Ag and Mg10Gd, were used to investigate the degradation behaviour in growing Sprague-Dawley® rats in a long-term study of 36 weeks. *In vivo* medium resolution μCT scans were performed at 1, 4, 12, 24 and 36 weeks post-operative to observe the longitudinal degradation of each alloy within the same animal. Moreover, *ex vivo* high resolution μCT scans and the corresponding bone sections stained with Toluidine Blue-O were conducted at 1 and 24 weeks after the operation. Additionally, Mg and Gadolinium (Gd) elemental distribution within the organs was studied at 4, 12, 24 and 36 weeks.

Results All the performed stainings worked properly at Technovit 9100 New embedded samples. Moreover, a slower degradation of pure Mg and Mg2Ag in comparison to the fast disintegrating Mg10Gd was displayed. Pure Mg and Mg2Ag were well integrated and surrounded by bone tissue 24 weeks after implantation. Both of these alloys showed no adverse reactions to the bone during their moderate degradation. On the contrary, Mg10Gd remnants, appearing 12 weeks post-operative, disturbed the bone remodeling until the end of the study because of its fast disintegration. The distribution of Mg and Gd elements showed that Gd

was accumulated especially in spleen, lung, liver and kidney rat organs even 36 weeks post-operative, whereas, no accumulation of Mg and Gd ions was observed in blood serum samples.

Discussion Histological analysis of the bone tissue embedded in Technovit 9100 New can provide detailed information about the real *in vivo* conditions on a cellular level. Mg10Gd induces less beneficial tissue reactions, while Mg2Ag showed moderate and adequate biodegradation and no adverse reactions in bone healing process which might be promising as an orthopaedic device. It is also shown that more extended studies regarding the biodegradation of the Mg alloys in parallel with the distribution of the alloying elements in organs and blood serum are necessary.

Zusammenfassung

Einleitung Materialien aus biodegradierbarem Magnesium (Mg) wurden auf ihre Eigenschaften für orthopädische Produkte untersucht. Unterschiedliche chemische Elemente wie zum Beispiel Seltene Erden werden oft als Legierungselemente den Mg Legierungen zu gemischt um die mechanischen Eigenschaften und die Degradationsbeständigkeit zu verbessern. Speziell für die mögliche Anwendung bei kindlichen Knochenbrüchen müssen Fragen nach deren Anwendbarkeit und Sicherheit geklärt werden. In den meisten Studien werden die Degradationseigenschaften und Biokompatibilität der Mg Legierungen *in vivo* mit micro-focused Computer Tomography (µCT) untersucht. Zusätzlich kann man über histologische Analysen in der neuen Technovit 9100 New Einbettungsmethode weitere und detailliertere Informationen erlangen wie und ob das Degradationsverhalten die Knochenzellen während des Heilungsprozesses beeinflussen kann.

Material und Methoden Die Epiphyse des distalen Femur wurde verwendet, um histologische Protokolle für die Einbettung von Rattenknochen in Technovit 9100 New zu etablieren. Zylindrische Pins von reinem Mg (99,99%) und zwei binären Mg Legierungen, Mg2Ag und Mg10Gd, wurden benutzt, um das Degradierungsverhalten in wachsenden Sprague-Dawley® Ratten in einer langfristigen Studie über 36 Wochen zu untersuchen. Nach 1, 4, 12, 24 und 36 Wochen. *In vivo* microCT Scans mittlerer Auflösung wurden bei 1, 4, 12, 24 und 36 Wochen postoperativ durchgeführt, um die longitudinale Degradierung von jeder Legierung innerhalb desselben Tiers zu beachten. Außerdem wurden ex vivo microCT Scans hoher Auflösung durchgeführt und die gleichen Knochen Schnitte wurde mit Toluidin Blue-O 4 und 24 Wochen nach der Operation gefärbt. Zusätzlich wurde die Verteilung von den Mg und Gd Elementen innerhalb der Organe 4, 12, 24 und 36 Wochen nach der Operation untersucht.

Resultate Die Färbungen der in Technovit 9100 New eingebetteten Proben konnten etabliert werden. Zusätzlich konnte eine langsamere Degradation von reinem Mg und Mg2Ag gegenüber dem schnell zerfallendem Mg10Gd gezeigt werden. Reines Mg und Mg2Ag wurden nach 24 Wochen gut in den Knochen

eingebaut. Beide Legierungen wiesen keine nachteiligen Reaktionen auf den Knochen auf während sie moderat im Knochen degradierten. Im Gegensatz dazu stören die desintegrierten Mg10Gd Reste die 12 Wochen nach der Operation aufgetaucht sind bis zum Ende der Studie nach 36 Wochen den Remodelling Prozess des Knochens. Diese Mg10Gd Stücke sind umgeben von fibrösem und knochigem Gewebe. Zusätzlich dazu wurde die Mg und Gd Ionen Konzentration in Organ- und Blutproben untersucht. Die Ergebnisse zeigten, dass Gd speziell in Milz, Lunge, Leber und Niere der Ratte nach 36 Wochen nach der Operation noch akkumuliert ist, wobei die Blutproben keine Akkumulation von Gd oder Mg Ionen aufwiesen.

Diskussion Histologische Analysen der Knochenproben eingebettet in Technovit 9100 New können sehr detaillierte Informationen über die realen in vivo Gegebenheiten auf zellulärer Ebene zur Verfügung stellen. Mg10Gd induziert weniger positive Gewebereaktionen, obwohl Mg2Ag gemäßigte und ausreichende Biodegradation und keine nachteiligen Reaktionen im Knochenheilungsprozess gezeigt hat, was für ein Osteosynthese versprechend sein könnte, ist die Biokompatibilität bezogen auf zugefügte Elemente im Kindesalter fraglich. Es wird auch gezeigt, dass Langzeit-Studien bezüglich der Biodegradation der Mg-Legierungen parallel zu der Ionen Konzentration von den Legierungselementen in Organen und Blutserum notwendig sind.

1 INTRODUCTION

1.1 Biodegradable Mg alloys

In the last years, biodegradable materials are studied because of their promising properties for biomedical applications such as vascular stents or orthopaedic implants. Due to the high biocompatibility, osteoinductivity and low stress shielding, because of an elastic modulus which is similar compared to bone tissue (4, 5), Mg gained more and more interest. Bioresorbable Mg implants are furthermore promising to be used in patients with bone fractures as no second surgery for the implant removal is necessary due to its degradation properties (6). However, Mg implants have to be considered for their usage as medical device because they can display uncontrolled and high degradation rates. As a consequence of too fast degradation, high amounts of hydrogen gas are released, and the pH and the ion concentrations of Mg increase in the surrounding tissue. These unwanted chemical effects can be reduced by different strategies such as by the usage of alloying elements or by tailoring the microstructure or by changing and modifying the implants' surface (4, 7).

Moreover, different elements in Mg alloys production and surface treatments (solution treatment-T4 and ageing treatment-T6) can be used in order to improve the corrosion properties of these implants (8). Various ways in alloys processing and surface treatment can be applied during their production. Diversity in shape and design of Mg implants such as screws, plates, discs or pins were applied and studied (2, 3, 6, 7, 9).

A strategy of decreasing the high degradation rates of Mg is the usage of alloying elements, which can influence the degradation rate and as a result, can guarantee the fracture stability for the required time of bone healing. The microstructure and thus the degradation rate can be tailored by alloying and/or heat treatment or using wrought materials. Suitable chemical elements such as aluminium (Al), zinc (Zn), manganese (Mn), calcium (Ca), zirconium (Zr) and REE are used to enhance the mechanical and physical properties of Mg alloys (10). The degradation performance of various Mg alloys has been investigated in *in vitro* or in *in vivo* conditions, however only few were performed with the same material. Even less

has been tested in both *in vitro* and *in vivo* conditions to compare their degradation behavior (11). On the one hand, degradation profiles were studied in *in vitro* conditions using immersion tests (12). Furthermore, cytotoxicity and biocompatibility can be examined using either primary cells (13) or different cell line cultures (8, 14). On the other hand, the degradation profile in *in vivo* conditions was studied using the non-destructive method of micro-computed tomography (μCT) and analyzing the material volume during the bone healing process (6, 7, 15).

In many cases, the alloys' compositions contain more than one alloying element in order to obtain more flexibility in terms of processing parameters, degradation and mechanical properties (16, 17). In other cases, Mg binary alloys are used in order to discover the effect of only one element in the biological *in vitro* system and these results can be used as guidance for future selection of the alloying elements to produce Mg alloys (3, 15).

Different chemical elements can be used as alloying elements to enhance the mechanical and physical properties of the Mg alloys (10). Zn, Mn and Ca enhance the mechanical properties of the implants and show non-toxicity and higher biocompatibility to the bone tissue. More specific, Mn is added to improve the corrosion resistance of the Mg alloys. Mn is also an important biological trace mineral, which plays a key role in cellular systems, and especially as cofactor for many metalloenzymes such as DNA and RNA polymerases, dehydrogenases and oxidases, kinases, decarboxylases and sugar transferases. Zn is added to the Mg alloys in order to reduce the hydrogen gas which is released during the degradation of the Mg alloys (18). Low amount of Zn results in high H_2 gas evolution during degradation in simulated body fluids, whereas Zn-rich alloys hardly form any hydrogen gas (18). From a biological point of view, Zn is an essential trace element, which is normally found in the body and is excreted mainly via the feces. It plays a key role in many processes such as nucleic acids and protein synthesis, carbohydrate and lipid metabolism (19). Ca is another element which is used in Mg-based materials. Ca is one of the main elements which can be found in bone and is beneficial to bone growth (20). Moreover, Ca can improve the corrosion resistance of Mg-based alloys (5).

Aluminium is a major alloying element in Mg-based alloys and is considered to enhance the strength and corrosion resistance. However, it has poor biocompatibility, which causes phosphate depletion in tissues. High concentrations of Al are considered to be neurotoxic and implicated in several pathologies such as dementia, senile dementia and Alzheimer's disease (19).

Zirconium is added as a grain refiner in Mg-based alloys but it has been linked to breast and lung cancer. REE are also considered to enhance the mechanical properties of the alloys but their toxicity in Mg-based materials is still questionable (5):

1.2 Methods of studying the degradation and the biocompatibility of the biodegradable Mg alloys during the bone healing process

In general, there are two different methods to investigate the osteoconductivity and biocompatibility of Mg alloying implants during the bone healing process. These methods are: the μCT and the immunohistochemistry. Moreover, the elemental distribution analysis of the Mg-based alloys materials would be one more method to investigate the biocompatibility of the bioresorbable Mg alloys.

1) μCT

Many studies investigate the degradation behavior of different resorbable Mg-alloys during bone healing. In most of them, μCT has been used in order to evaluate their degradation process and their biocompatibility during the bone healing process (3, 6, 7). Tomography is a method which is widespread used for imaging of implanted materials in bones of different animals such as mice (21),

rats (3, 6, 7, 12, 22), rabbits (23, 24) and sheep (25, 26). Volume and surface of the materials, as well as the formed gas due to their degradation, can be evaluated through the usage of specific software.

μCT is a non-invasive method, which is used to provide quantitative and qualitative 3-dimensional (3D) information of bone architecture. μCT can be used for both *in vivo* and *ex vivo* experimental applications.

Advantages of *in vivo* μCT

- Imaging is performed on the same alive small animal, which is under anesthesia, at different time points. As a result, the longitudinal observation of bone and implant changes of the same animal can be performed.
- Radiation dose levels, in which the animals are exposed to, are low.
- Qualitative analysis of bones and materials' inserts during the *in vivo* study can be performed.
- Quantitative analysis of implant volume, implant surface, gas volume, bone mass and bone density can be also performed.
- 3D models of the bone samples can be produced.
- Transformation of the image datasets files into DICOM format for further *in-silico* applications.

Advantages of *ex vivo* μCT

- High resolution imaging of small bone samples
- Qualitative analysis of bones and materials' inserts in more details can be performed.
- Quantitative analysis of implant volume, implant surface, gas volume, bone mass and bone density can be also performed.
- Histology of the bone samples can be performed after the completion of the scanning.

However, less is known about how bone reacts after the implantation with a biodegradable Mg alloy and during the bone healing process on a molecular level. For this reason, during the last decades many studies have been performed in order to investigate more histological methodologies, which can be used in materials' science field.

2) Immunohistochemistry

Immunohistochemistry is a method that could be used for further investigation of cell reactions during bone healing procedure after the material implantation.

Various bone tissue embedding methods are used in order to analyze and evaluate the efficiency and the effects of the Mg bioresorbable materials on the bone growth and bone healing process (27, 28). The most widespread embedding methods use paraffin, Technovit 7200 and Technovit 9100 New. In this thesis, a short comparison between paraffin and Technovit 9100 New has been performed.

Paraffin is commonly used for the histology of soft embedded tissues. This method can be also used for embedding hard tissues such as bone and teeth but these tissues need to be decalcified before their embedding (28). Furthermore, undecalcified bone or teeth samples which are implanted with titanium, steel or Mg biodegradable materials cannot be embedded in paraffin because paraffin is not a hard embedding method and cannot provide thin or semi-thin sections. In this case, the materials need to be removed before the fixation, which may cause the loss of bone, which surrounds the material surface and, as a result, can cause the possible destruction of the bone-implant interface. Moreover, decalcification steps could cause the loss or damage of the epitopes (27).

Technovit 9100 New is a very promising embedding method which is especially used for hard tissue such as bone and teeth which are implanted with bioresorbable Mg alloys or biodegradable polylactide/polyglycolide-based implants (27). Hard tissues which are implanted with permanent implants such as titanium-

or stainless steel-based implants can be also embedded in Technovit 9100 New but the implants need to be electrochemically removed before cutting of these samples in thin sections (29). The main advantages of Technovit 9100 New embedding method, used in bone tissues which are implanted with bioresorbable Mg alloys, are that: decalcification steps and removal of the Mg-alloy implants are not necessary. Technovit 9100 New can be used for general stainings, enzyme-based histochemistry and immunohistochemistry (30) because the polymerization of the samples takes place at low temperature.

3) Distribution of the alloying elements

Instead of the µCT and immunohistochemistry methods, the biocompatibility of Mg alloys can be also investigated through the elemental distribution of the alloying elements. The ions which are released due to the degradation of the Mg alloys can be accumulated within the organs and can cause systemic toxicity to the organism (31). Until today, there are a lot of *in vitro*-cytotoxicity studies which investigate the toxicity of different elements on various cells (14, 32-39). In addition, there are *in vivo* studies in which the biocompatibility is investigated through histology at tissue sites which are close to the implant material (6, 12, 40-43). However the distribution of various alloying elements within the body and possible systemic effects have not been published yet (44). Elemental distribution in various tissues as well as blood serum elemental concentration studies could elucidate the pathways of the metabolism of these alloying elements. As a result, safer conclusions could be deduced regarding the biocompatibility and safety of the studied materials.

1.3 Aims of this thesis

The aims of this thesis are divided into three parts:

a) Part 1: Establishment of the Immunohistochemistry in Technovit 9100 New

b) Part 2: *In vivo* degradation of binary Mg alloys – a long-term study

c) Part 3: Elemental distribution of a REE-containing Mg alloy

2 Part 1: Establishment of the Immunohistochemistry in Technovit 9100 New

2.1 Aim of this part

Technovit 9100 New embedding method has already used in rabbit bone tissue (27), in human bone tissues (45) and in ovine or bovine trabecular bone (30). The aim of the first part of this thesis was to establish the immunohistochemistry in Technovit 9100 New embedding method for rat bone tissue in our lab. For this purpose, distal epiphysis bone tissues from male growing Sprague-Dawley rats, which were implanted with cylindrical pins (length of 8 mm and diameter 1.6 mm) of bioresorbable Mg alloys, were used. Different kind of general stainings and immunostainings were performed.

2.2 Materials and Methods

The bones from male growing Sprague-Dawley rats (age: 5-6 weeks, weight: 140-170 g) were used for the establishment of the immunohistochemistry in Technovit 9100 New embedding method. The cylindrical pins (8 mm length and 1.6 mm diameter) were implanted in the trans-epiphyseal growth plate of the distal femoral bone (Figure 2.1).

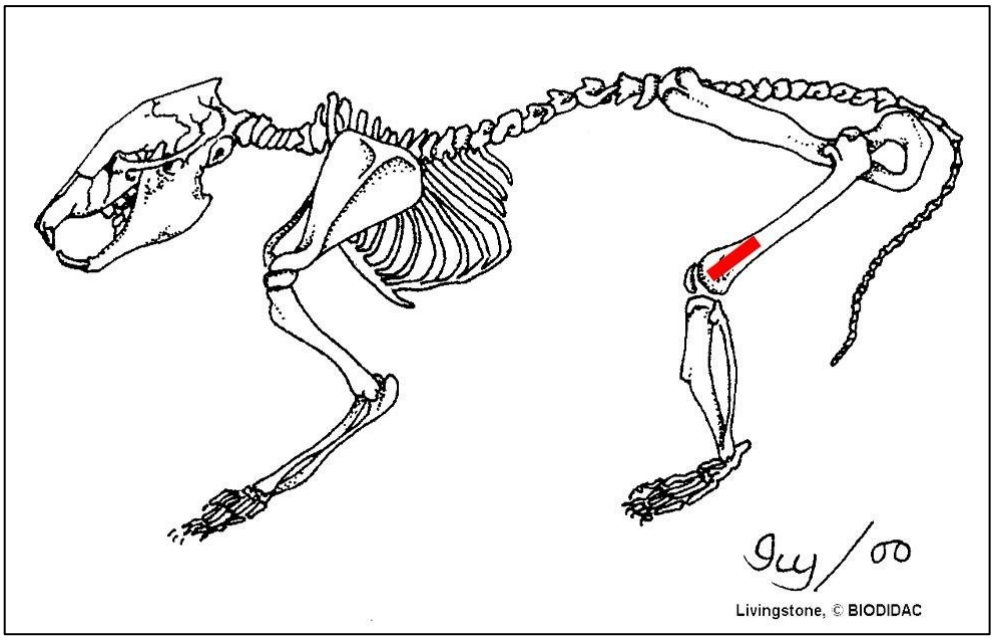

Figure 2.1: Trans-epiphyseal growth plate animal model (1).

2.2.1 Technovit 9100 New embedding method procedure

Four and twenty-four weeks after the implantation, the bones were explanted and were scanned in µCT with a high resolution protocol. The bone samples were embedded in Technovit 9100 New (Heraeus Kulzer, Wehrheim, Germany) method, which is described by Willbold and Witte (27). The bones were cut into the proper size and put in the embedding cassettes in brown-light protective bottles. The bones were fixed in Formalin 3.7 % for 48 h and then dehydrated with different grades of isopropanol and xylol. The probes were dehydrated twice in 70 % isopropanol for 4 h each and once in 70 % isopropanol overnight; twice in 70 % isopropanol for 4 h each and once in 70 % isopropanol overnight; twice in 96 % isopropanol for 4 h each and once in 96 % isopropanol overnight; twice in 100 % isopropanol for 4 h each and once in 100 % isopropanol overnight; twice in 100 % isopropanol for 4 h each and once in 100 % isopropanol overnight; twice in xylol for 4 h each and once in xylol overnight; twice in xylol for 4 h each and once in xylol overnight. During each dehydration step, the liquids in glass bottles including

the embedding cassettes had to be evacuated immediately after every exchange of a solution for at least 10 min and gently shaken to remove all gas from the liquid and the embedding cassettes. After the dehydration steps, the probes were covered with pre-infiltration solution for 3 days at 4 ^{o}C, afterwards with the infiltration solution for 7 days at 4 ^{o}C. Then the probes were polymerized with the polymerization solution (Stock solution A and B in 9:1 ratio) at -4 ^{o}C for 5 days. The probes were put in cool embedding forms (stayed overnight at 4 ^{o}C), covered with the polymerization solution, evacuated for at least 10 minutes and put at 4 ^{o}C. The polymerization procedure of the samples takes place at -4 ^{o}C for 5 days.

After the polymerization, the blocks have to be put under the laboratory fume hood, overnight, in order to be totally evaporated.

The bone samples were cut in 5 µm slices using a rotation microtome (Histocom, HM 355 S, Vienna, Austria) with a specific D knife (Histocom, 152120, Vienna, Austria) and dried at 37 °C for 3 days.

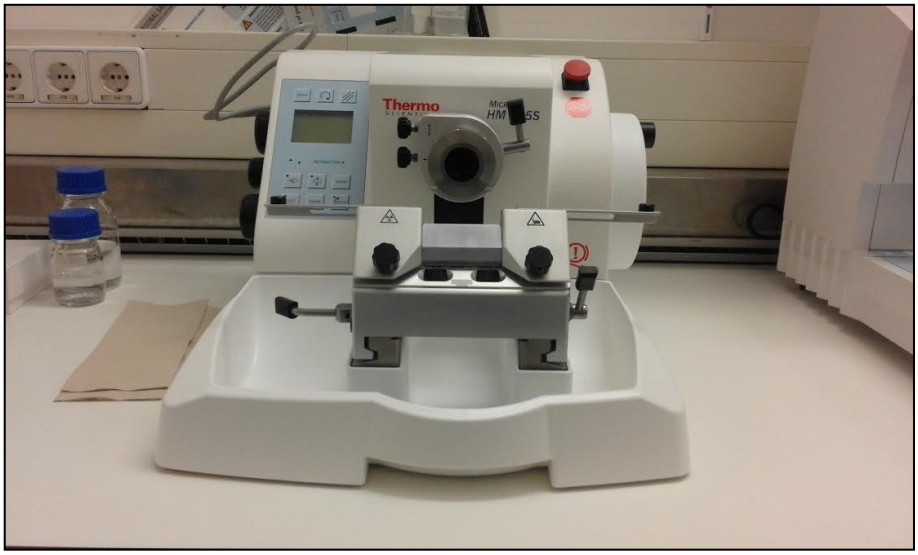

Figure 2.2: Rotation microtome used for cutting Technovit 9100 New embedded bone samples.

2.2.2 Paraffin embedding method procedure

The paraffin samples used for in this study were decalcified and embedded in paraffin by Gudrun Sonderegger, Medical University Graz. The bones were fixed in 4 % Formalin for 48 h and then were decalcified in 12.5 % ethylenediaminetetraacetic acid (EDTA) + 1.25 % sodium hydroxide (NAOH) (both from Sigma-Aldrich, Vienna, Austria) for approximately 8 weeks. Then, the specimens were washed overnight, dehydrated with different grades of ethanol (30 %, 50 %, 70 %, 96 % and 100 %), cleared in xylol and embedded in paraffin (46).

The bone tissues were cut in 5 µm thickness with a rotation microtome with a specific blade for hard tissues and, afterwards, well-dried overnight at 37 °C.

Figure 2.3: Rotation microtome used for cutting paraffin embedded bone samples.

2.2.3 Deplastification and rehydration

Before the slices can be stained, the bone tissue sections embedded in Technovit 9100 New have to be deplastified and the bone tissue sections embedded in paraffin have to be deparaffinised.

The deplastification process of Technovit 9100 New embedded tissue included the following steps:

- 2x in Xylol for 10 min
- 1x in MEA (2-methoxyethyl acetate, Merck, Vienna, Austria) for 10 min
- Rehydration in a graded series of isopropanol (100%, 100%, 96%, 70%) for 2 min at each step
- 1x distilled water for 2 min

The deparaffinisation process of paraffin embedded tissue included:

- initially the sections were put at 60 ^{o}C for 30 min
- 2x in Xylol for 10 min
- 1x in xylol/ethanol for 3 min
- Rehydration in a graded series of ethanol (100%, 96%, 70%) for 3 min at each step
- 1x in distilled water for 5 min

2.2.4 Stains

The stainings which used for this aim of the study were:

1) Stainings performed in rat bone tissues embedded in Technovit 9100 New and in paraffin: general stainings like toluidine blue-O and Hematoxylin-Eosin (HE), and immunohistochemical stainings like collagen II and osteocalcin.

2) Stainings performed in bone tissues embedded in Technovit 9100 New: general stainings like safranin-O and Movat's Pentachrome, enzyme based histochemical stainings like Tartrate Resistant Acid Phosphatase (TRAP) and chloracetatesterase and immunohistochemical stainings like collagen I.

2.2.4.1 Stainings performed in bone samples embedded in Technovit 9100 New and in paraffin

Toluidine Blue-O

After the rehydration steps, the sections embedded in Technovit 9100 New were stained with 0.1% toluidine blue-O (Sigma, Vienna, Austria) for 40 s, washed in distilled water, dehydrated with a series of isopropanol and xylol and mounted in Eukitt® (Sigma-Aldrich Handels-GmbH, Vienna, Austria).

The sections embedded in paraffin, were stained with 0.1% toluidine Blue-O for 30 s, washed in distilled water, dehydrated with a series of isopropanol and xylol and mounted in Eukitt®.

Hematoxylin-Eosin

After the rehydration, the sections embedded in Technovit 9100 New were incubated for 8 min with Mayer's hematoxylin, rinsed in tap water for 10 min, stained with 1 % eosin (Merck, Vienna, Austria) for 5 min, dehydrated in a graded series of isopropanol and xylol and mounted in Eukitt®.

The sections embedded in paraffin, were incubated for 2 min with Mayer's hematoxylin, rinsed in tap water for 3 min, stained with 1 % eosin for 30 sec, dehydrated in a graded series of ethanol and xylol and mounted in Eukitt®.

Immunohistochemistry with Collagen II and Osteocalcin

Generally, the rehydrated sections were first mildly digested for antigen retrieval with proteinase K (Dako, Vienna, Austria) for 20 min at 37 ^{o}C for Technovit 9100 New embedded tissues and 7 min for paraffin embedded tissues, followed by washing steps in Tris-buffered saline (TBS) twice, 5 min each wash. After washing in TBS, sections were pre-incubated with a solution of 0,3 % H_2O_2 in TBS for 30 min to block endogenous peroxidase activity and then were washed in TBS twice (5 min each step). Afterwards, the sections were incubated for 30 min in a solution of 10 % normal goat serum derived from the host species of the secondary antibody (Vector/ZABO-SCANDIC HandelsGmbH, Vienna, Austria) in TBS to block unspecific antibody binding. Then the sections were incubated with the primary antibody for 60 min at room temperature. The antibodies used were mouse anti-collagen II (Acris, Vienna, Austria) and mouse-anti-osteocalcin (LSBC-73941, eubio, Vienna, Austria). The dilution of collagen II antibody for Technovit 9100 New embedded tissues was 1/100 and for paraffin 1/200. The dilution of osteocalcin antibody for Technovit 9100 New embedded tissues was 1/1000 and for paraffin 1/500. The sections were washed twice in TBS (5 min each), followed by a peroxidase-labelled secondary antibody (goat-anti-mouse-EnVision, Dako, Vienna, Austria) for 30 min at room temperature. Peroxidase activity was visualized using the liquid diaminobenzidine (DAB) substrate chromogen system (Dako). Sections were then washed twice with TBS and distilled water, stained with Hematoxylin which was used as the counterstain and finally mounted in Aquatex® (Merck, Vienna, Austria). As negative controls, the primary antibody was omitted. No staining was seen in these sections.

2.2.4.2 Stainings performed in bone samples embedded in Technovit 9100 New

Safranin-O

After the rehydration steps, the sections were stained with 0.05 % safranin-O (Sigma; Vienna, Austria) for 4 min, washed in distilled water, dehydrated with a series of isopropanol and xylol and mounted in Eukitt®.

Movat's Pentachrom

After the rehydration, the sections were rinsed in 3 % acetic acid for 30 s, incubated in Alcian Blue for 30 min and washed in tap water for 2 min. Afterwards, the sections were incubated in Verhoeff's solution for 6 min and were washed in distilled water. For differentiation, the sections were incubated in 1 % ferric chloride solution and then were washed in distilled water to stop the differentiation. Then the sections were incubated in Brilliant Crocein Acid fuchsin for 6 min and were rinsed in 1 % aqueous acetic acid. After these steps, they were incubated for 15 min in 2 % tungstophosphoric acid and were rinsed in 1 % aqueous acetic acid. The dehydration steps were done with Ethanol 99%, isopropanol and xylol and then the sections were mounted in Eukitt®.

Tartrate-resistant acidic phosphatase (TRAP)

Rehydrated sections were first placed in 0.2 M acetate buffer for 20 min and then in freshly prepared TRAP staining solution which contains naphtol-AS-MX phosphate sodium salt and Fast Red TR salt in 0.2 M acetate buffer (all from Sigma, Vienna, Austria) for 120 min. After staining, the sections were washed in distilled water and mounted with Aquatex® (Merck, Vienna, Austria). Control sections were incubated in a solution that does not contain the substrate. No staining developed in these control sections.

Chloracetatesterase

The rehydrated sections were firstly washed twice in Phosphate-buffered saline (PBS) for 5 min each. Then the sections were decalcified in EDTA buffer for 60 min at 37 ^{o}C followed by 3 washing steps in distilled water for 2 min each step. Afterwards, the sections were incubated with naphthol-AS-D-Chlor-acetate (Sigma, Vienna, Austria) in 4 % pararosanillin (Chroma) and 4 % sodium nitrate (Merck, Vienna, Austria) in PBS-Buffer for 2h. Sections were washed twice in distilled water for 3 min each and mounted with Aquatex® (Merck, Vienna, Austria). All cells containing reddish-brown granules were regarded as positive. Control sections were incubated in incubation solution that did not contain the substrate. No staining developed in these control sections.

Immunohistochemistry with Collagen I

Generally, the rehydrated sections are first mildly digested for antigen retrieval with proteinase K (Dako, Hamburg, Germany) for 20 min at 37 ^{o}C, followed by washing steps in TBS twice, 5 min each. After washing in TBS, sections are preincubated with a solution of 0.3 % H_2O_2 in TBS for 30 min to block endogenous peroxidase activity and then washing steps in TBS twice, 5 min each, are done. Afterwards, the sections are incubated for 30 min in a solution of 10 % normal goat serum derived from the host species of the secondary antibody (Vector/ZABO-SCANDIC HandelsGmbH, Vienna, Austria) in TBS to block unspecific antibody binding. Then the sections are incubated with the primary antibody for 60 min at room temperature. The antibody used was mouse anti-collagen I (Acris). The sections are washed twice in TBS (5 min each), followed by a peroxidase-labelled secondary antibody (goat-anti-mouse-EnVision, Dako) for 30 min at room temperature. Peroxidase activity is visualized using the liquid diaminobenzidine (DAB) substrate chromogen system (Dako). Sections are then washed twice with TBS and distilled water, stained with Hematoxylin which was used as the counterstain and finally mounted in Aquatex. As negative controls, the primary antibody was omitted. No staining was seen in these sections.

2.3 Results

Paraffin embedded method is widespread used in histological evaluation of soft embedded tissues. However, it can be hardly used for bone tissues which are implanted with Mg biodegradable materials. To keep the bone and implant intact and therefore to allow the analysis of the bone-implant interface these hard tissues can be embedded in Technovit 9100 New.

The establishment of the stainings of rat bone tissues embedded in Technovit 9100 New was one main part of this thesis. For this reason, distal femoral bones implanted in the epiphyseal growth plate with Mg alloy cylindrical pins, were used.

2.3.1 Stainings performed in bone samples embedded in Technovit 9100 New and in paraffin

The following stainings are routinely used in tissues which are embedded in paraffin. The already standardized stainings' protocols in paraffin embedded bone tissue were used as the basis for the establishment of the stainings' protocols in Technovit 9100 New embedded rat bone tissue.

Toluidine Blue-O

As one of the general stainings, toluidine blue-O shows the general bone morphology. Information regarding the old and the new bone (osteoid) as well as the osteoblasts and the osteocytes can be drawn out of using this staining. For this

reason, toluidine blue-O constitutes a good stain for detecting changes in bone morphology before and after implantation.

Toluidine blue-O worked both in Technovit 9100 New (Figure 2.4 A) and in paraffin (Figure 2.4 B) embedded bone tissue. The only difference between the protocol procedures is the incubation time needed for the bone sections remaining in the toluidine blue-O staining solution (40 s for Technovit 9100 New and 30 s for paraffin embedded bone tissue).

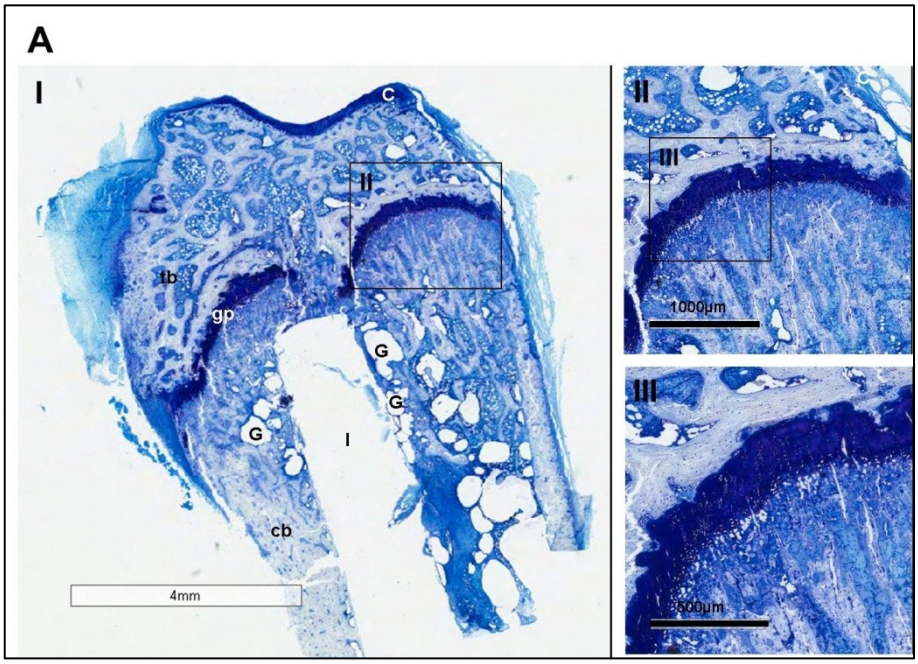

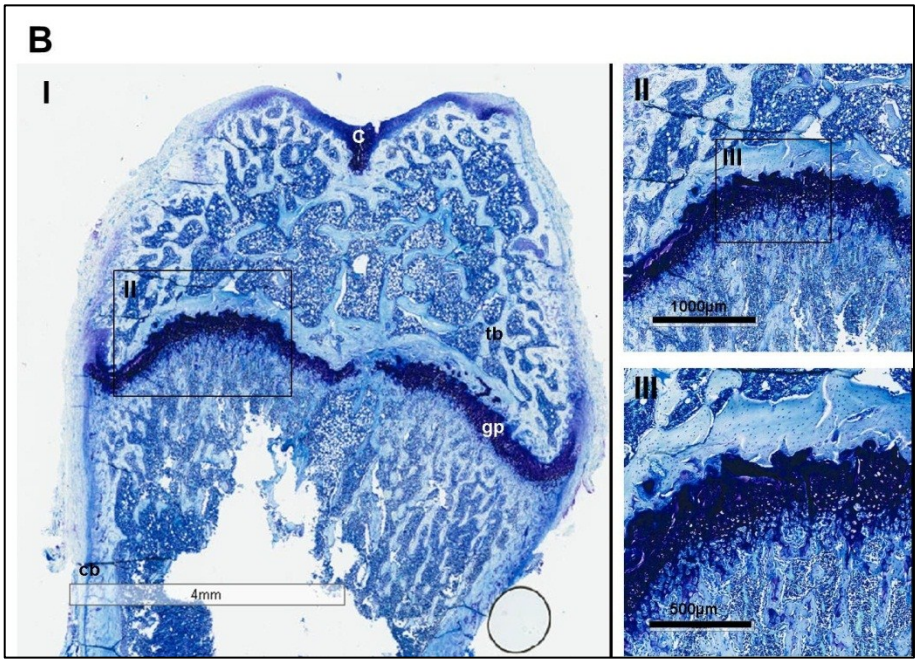

Figure 2.4: Toluidine Blue-O staining in bone tissue embedded in (A) Technovit 9100 New and in (B) paraffin. General bone morphology is shown (A-I and B-I): Growth plate is shown in higher magnification (A-II, A-III, and B-II, B-III), I: implant, tb: trabecular bone, cb: cortical bone, G: gas formation, C: cartilage, gp: growth plate.

Hematoxylin-Eosin (HE)

Hematoxylin-Eosin (HE) is a widely used staining in routine laboratories investigation. HE is a general staining which provides information about the general bone morphology. HE staining is detected in both Technovit 9100 New (Figure 2.5 A) and paraffin (Figure 2.5 B) embedded bone tissue. Growth plate and cartilage are stained in purple, cortical and trabecular bone is stained in pink. In higher magnification (Figures 2.5: A-III and B-III), the cells within the five zones of the growth plate are obvious. The HE staining protocols, which were followed for each embedding method, differed in incubation time that the bone sections needed to remain in the hematoxylin solution (8 min for Technovit 9100 New and 2 min for paraffin embedded bone tissue) and eosin solution (5 min for Technovit 9100 New and 30 sec for paraffin embedded bone tissue).

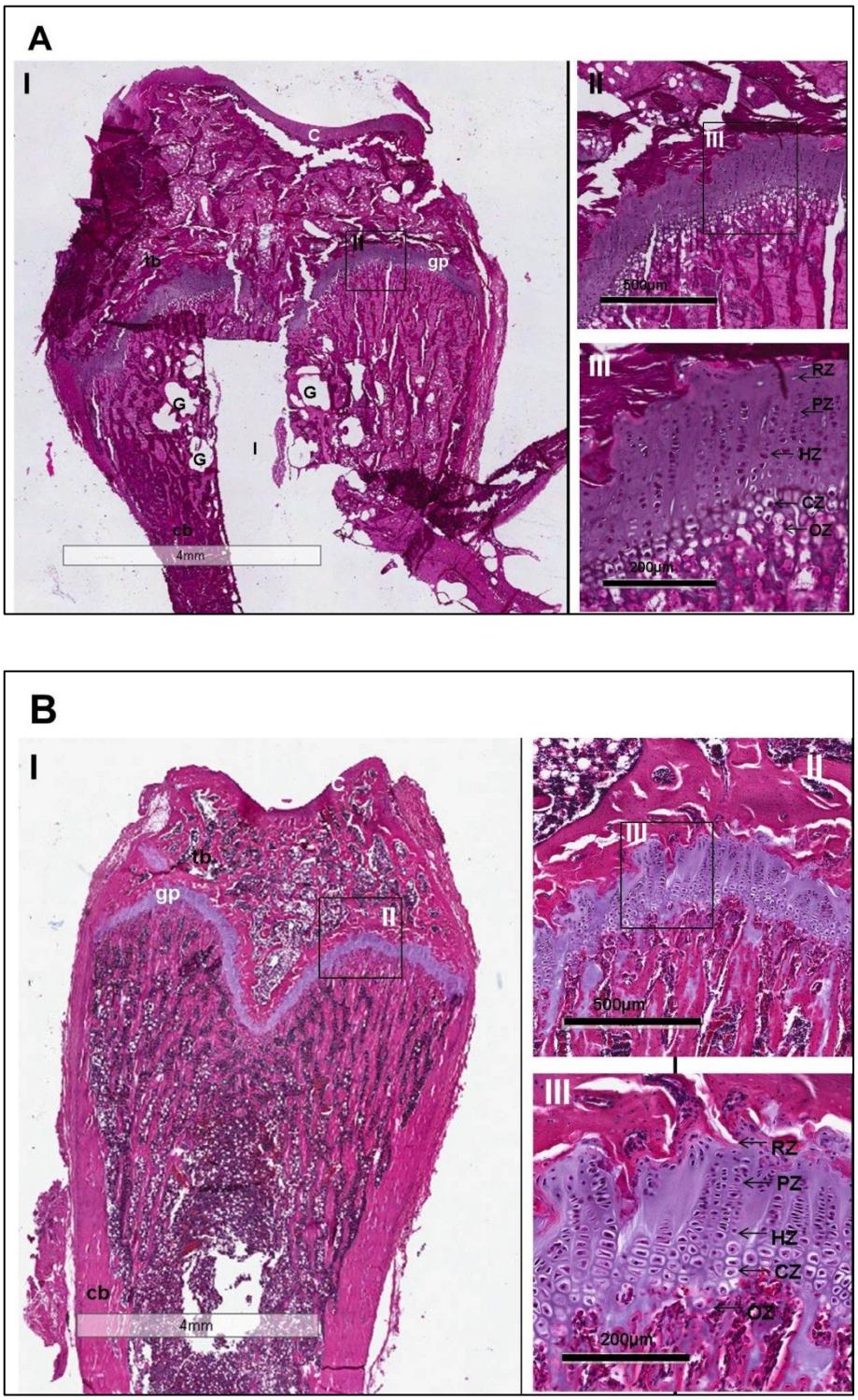

Figure 2.5: Hematoxylin-Eosin staining in bone tissue embedded in (A) Technovit 9100 New and in (B) paraffin. General bone morphology is shown (A-I and B-I): Growth plate is shown in higher magnification (A-II, A-III and B-II, B-III). In higher magnification (A-III and B-III), the five zones (RZ=Rest zone, PZ=Proliferation

zone, HZ=Hypertrophic zone, CZ=Calcified zone and OZ=Ossification zone) of the growth plate are visible. I: implant, tb: trabecular bone, cb: cortical bone, G: gas formation, C: cartilage, gp: growth plate.

Collagen II

Collagen type II is the main collagen which is found in cartilaginous tissues. The collagen II staining has been performed by applying an antibody detecting the cartilaginous tissues. It is expressed in the growth plate and the cartilage of the distal femoral epiphysis but it is absent in the cortical and trabecular bone. The collagen II antibody worked in both Technovit 9100 New (Figure 2.6 A) and paraffin (Figure 2.6 B) embedded bone tissues. In both embedding methods, bone tissue in which its incubation with the primary antibody is omitted (Figure 2.6: A-IV and B-IV) and kidney tissue in which its incubation with the primary antibody is done, (Figure 2.6: A-V and B-V) can be used as negative controls. In both cases, the sections are not stained. The differences between the staining protocols of the Technovit 9100 New and the paraffin embedded tissues are: 1) the incubation time of the bone tissues in Proteinase K antigen retrieval solution (20 min for Technovit 9100 New and 7 min for paraffin sections) and 2) the dilution of the primary anti-collagen II antibody (1/100 for Technovit 9100 New and 1/200 for paraffin embedded bone sections).

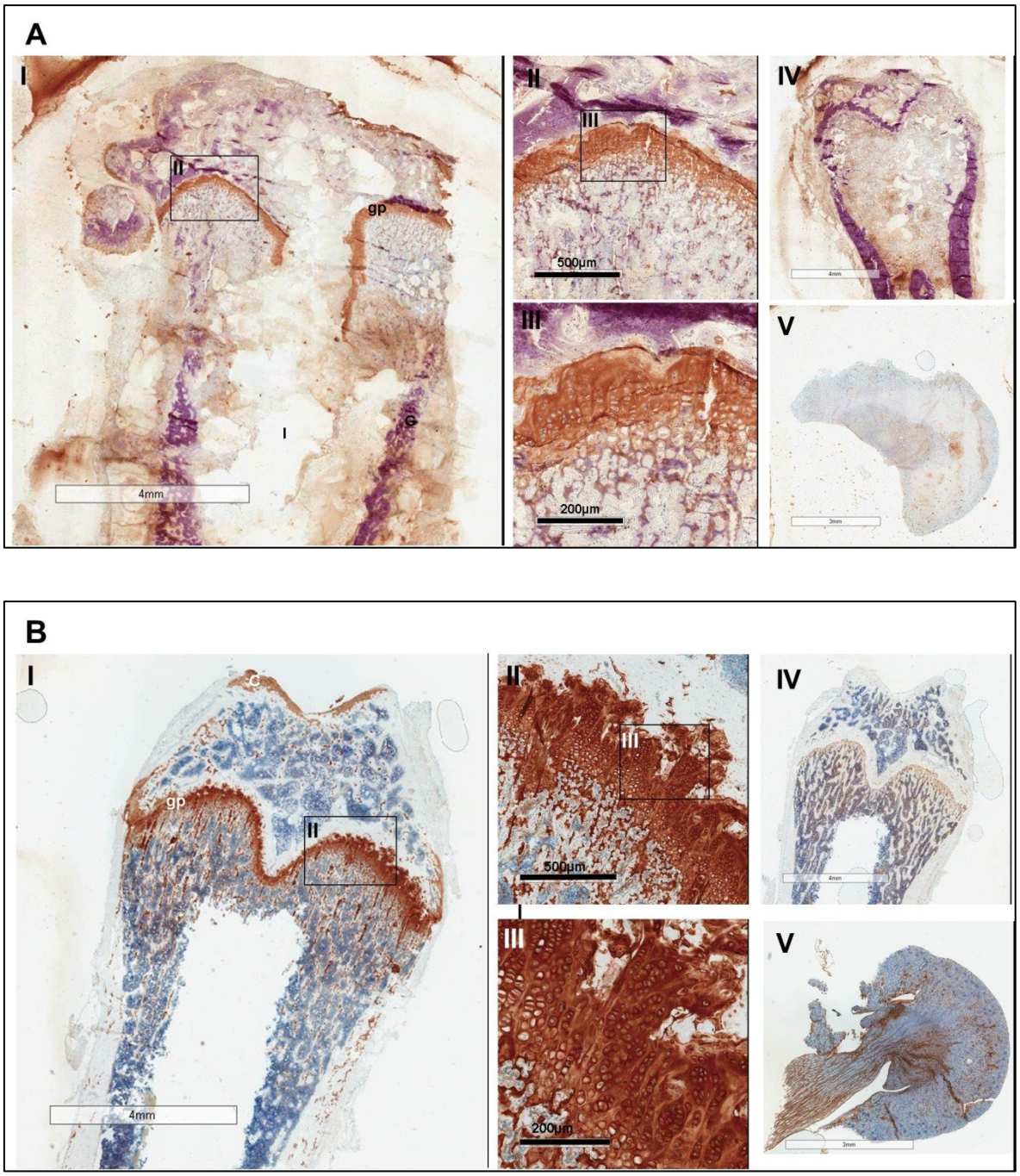

Figure 2.6: Collagen II antibody staining in bone tissue embedded in (A-I) Technovit 9100 New and in (B-I) paraffin. The growth plate is shown in higher magnification (A-II, A-III and B-II, B-III). Bone tissue in which the primary antibody's incubation has been omitted (A-IV and B-IV) and kidney tissue in which the primary antibody's incubation has been performed (A-V and B-V), can be used as negative controls, as the sections are not stained. I: implant, gp: growth plate, c: cartilage.

Osteocalcin

Osteocalcin is a non-collagenous protein which is detected in bone matrix. It is secreted by the osteoblasts. For this reason it is used as a marker of bone formation procedure. It worked in both Technovit 9100 New and paraffin embedded bone tissues (Figures 2.7 A and B, respectively). In both embedding methods, negative controls of bone tissues, in which their incubation with the primary antibody was omitted, were used (Figure 2.7: A-IV, B-III and B-IV). The difference between the staining protocols performed in Technovit 9100 New and in paraffin embedded bone slices was the dilution of the primary anti-osteocalcin antibody (1/1000 for Technovit 9100 New and 1/500 for paraffin embedded bone sections).

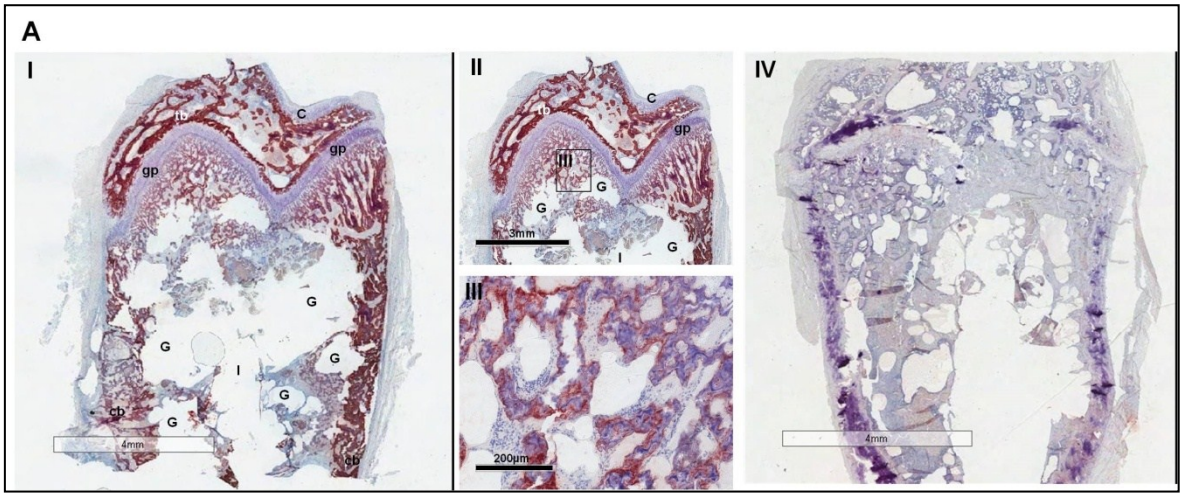

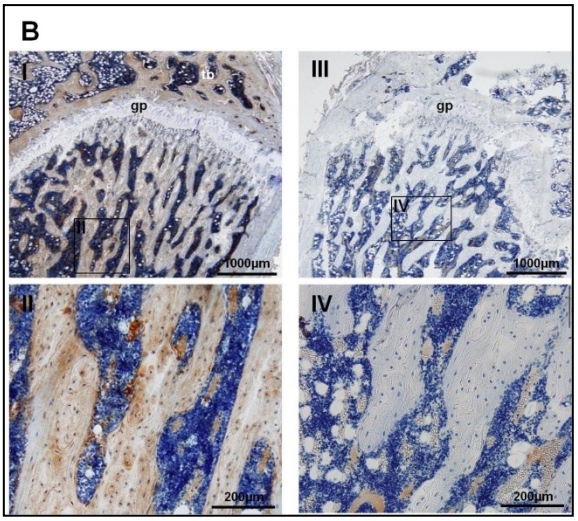

Figure 2.7: Osteocalcin antibody staining of bone tissue embedded in (A) Technovit 9100 New and in (B) paraffin. Bone tissue is shown in higher magnification (A-II, A-III and B-II, B-IV). Negative controls, where the primary antibody's incubation has been omitted, are displayed (A-IV, B-III and B-IV). I: implant, gp: growth plate, cb: cortical bone, tb: trabecular bone, G: gas formation.

2.3.2 Stainings performed in bone samples embedded in Technovit 9100 New

Safranin-O

Safranin-O staining is used to detect the cartilaginous tissues. This staining detects the growth plate and the cartilage of the bone which are colored in pink. This staining can provide information about the changes of the growth plate's morphology because of the insertion of a biodegradable implant (Figure 2.8-I).

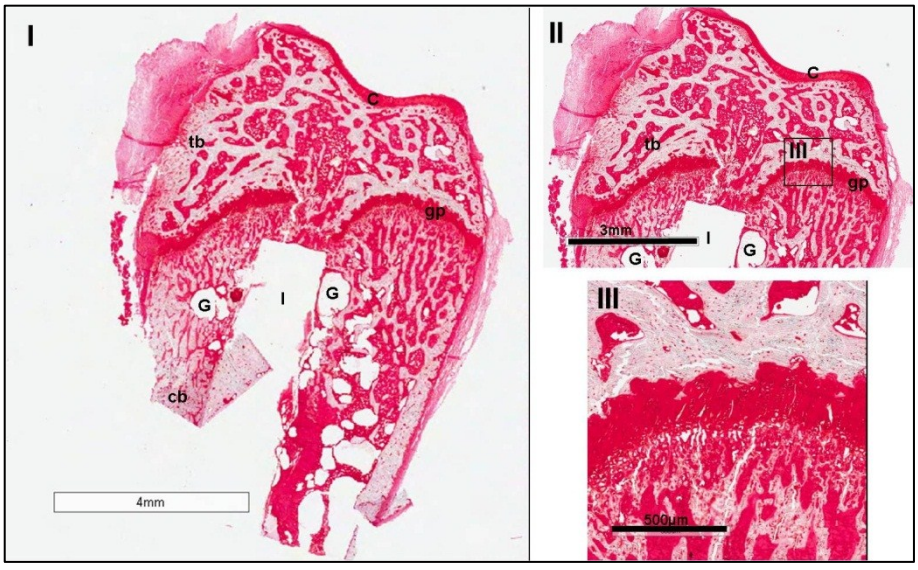

Figure 2.8: Safranin-O staining of bone tissue embedded in Technovit 9100 New. Growth plate and cartilage are detected (I and II): Growth plate is shown in higher magnification (III). I: implant, tb: trabecular bone, cb: cortical bone, G: gas formation, C: cartilage, gp: growth plate.

Movat's Pentachrome

The Movat's Pentachrome staining detects various tissue components in the same histological section. The 5 different solutions which are contained in the Movat's Pentachrome are: 1) Alcian Blue, which stains the cartilage 2) Verhoeff's solution which stains the nucleus, 3) 1% Ferric chloride solution which is used for the nuclei differentiation, 4) Brilliant Crocein Acid Fuchsin which stains the muscles and the non-calcified bone (osteoid) and 5) Safron du Gatinais solution which stains the connective tissue. Movat's Pentachrome staining is a staining which can also be used for the general bone morphology. In bone tissue, it can detect the growth plate, mineralized cartilage (green) and non-mineralized cartilage (blue), calcified bone (yellow) and non-calcified bone (osteoid, red), muscles (red), nucleus (red-brown). In higher magnification (Figure 2.9-II) the upper site of the growth plate, which is non-mineralized cartilage, is colored in blue, whereas the lower part of the growth plate, that it is getting mineralized cartilage, is colored in green. In Figure 2.9-III, the osteoid which is colored in red (small arrow), is found at the edge of the calcified bone (yellow, big arrow).

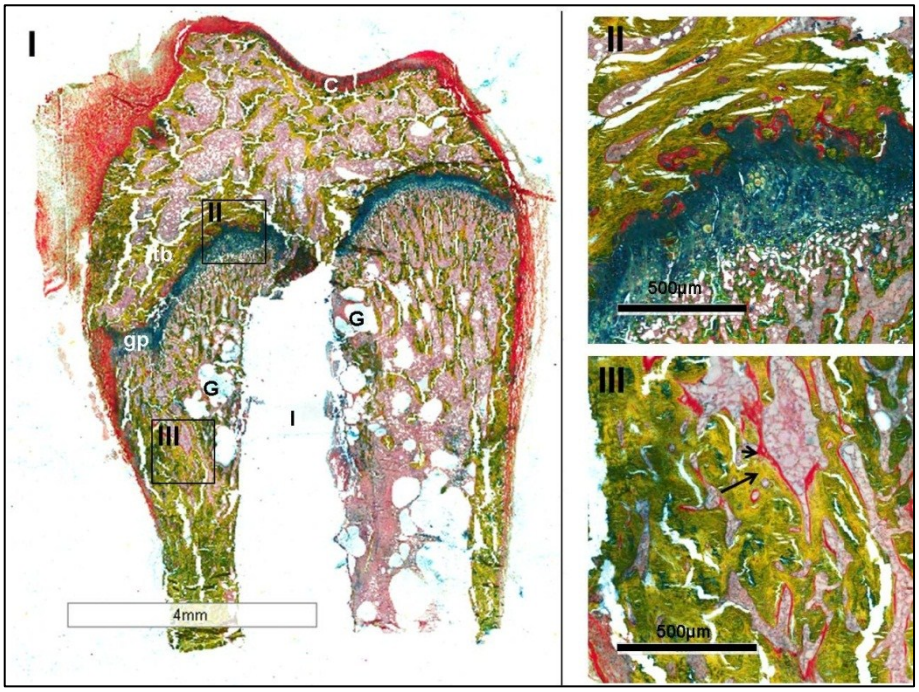

Figure 2.9: Movat's Pentachrom staining of bone tissue embedded in Technovit 9100 New. General bone morphology is shown in an overview (I). Bone tissue areas are shown in higher magnification (II and III). The osteoid which is colored in

red (small arrow) is found at the edge of the calcified bone (yellow, big arrow), (III). Movat's Pentachrom is a simple staining that can be used for general bone morphology. I: implant, Tb: trabecular bone, Cb: cortical bone, G: gas formation.

Tartrate Resistant Acid Phosphatase (TRAP)

TRAP staining is an enzyme-based histochemical staining (Figure 2.10-I). TRAP is expressed by osteoclasts which play a key role in the bone remodeling process. Trap staining can be used as a marker of bone resorption procedure. It is obvious that the osteoclasts are detected close to the growth plate (Figure 2.10-II) and also in the interface between the implant and the bone (Figure 2.10-III). The epiphysis of a young animal has been used as positive control (Figure 2.10-V and -V).

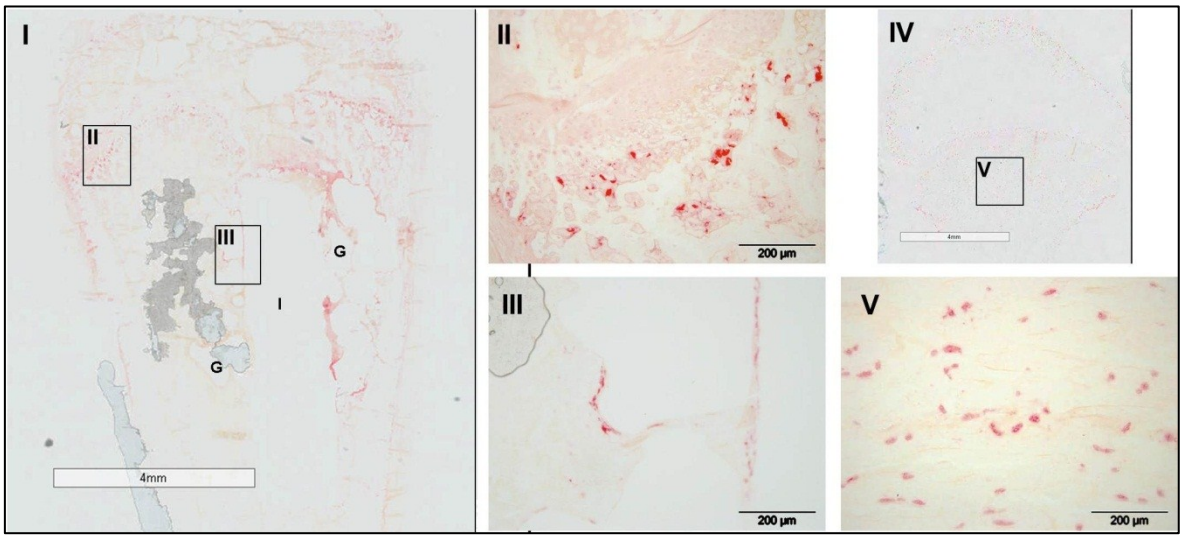

Figure 2.10: Tartrate-Resistant Acid Phosphatase (TRAP) staining in bone tissue embedded in Technovit 9100 New (I). In higher magnification, the region of the growth plate (II) and the implant-bone interface (III) are visible. The epiphysis of a young animal can be used as positive control (IV and V). I: implant, G: gas formation.

Chloracetatesterase

Chloracetatesterase staining is also an enzyme-based histochemical staining Chloracetatesterase stains the neutrophils and can be used as a marker of the inflammation status of the tissue. Neutrophils are stained in red and can be observed within the bone marrow (Figure 2.11-III, arrows). Spleen tissue has been used as positive control (Figure 2.11-IV) when it is incubated in substrate solution and as negative control (Figure 2.11-V) when it is not incubated in substrate solution.

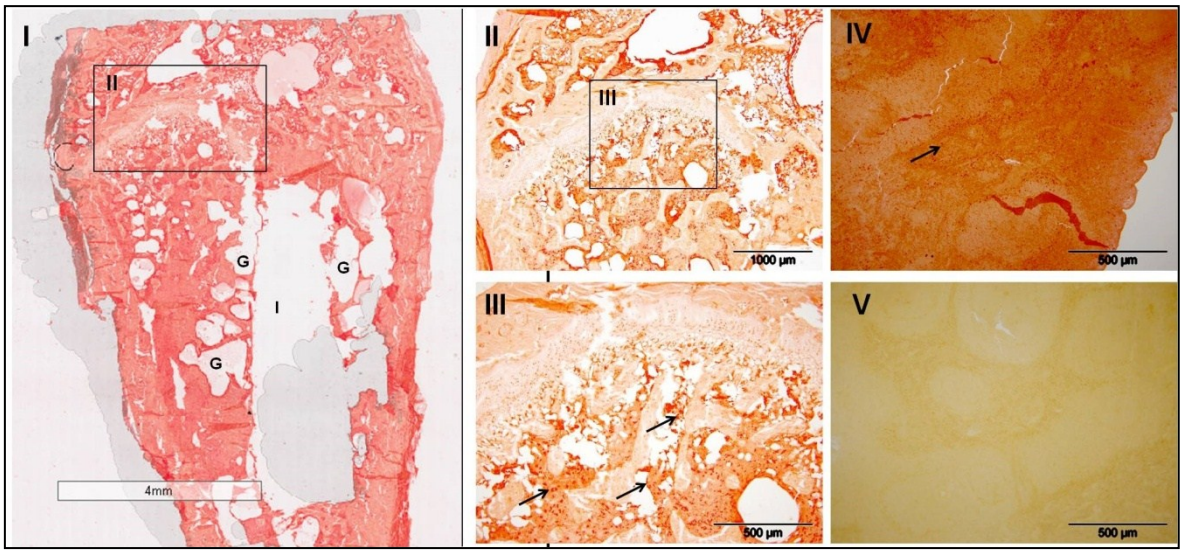

Figure 2.11: Chloracetatesterase staining in bone tissue embedded in Technovit 9100 New (I). An area of the bone tissue is shown in higher magnification (II and III). Spleen tissue, incubated in substrate solution, has been used as a positive control (IV), and with no incubation in the substrate solution, has been used as a negative control (V). I: implant, G: gas formation, arrows: neutrophiles stained in red.

Collagen I

Collagen I is the main component of the bone. Collagen I expression can be detected to cortical and trabecular bone whereas it is absent in cartilage and growth plate (Figure 2.12). Bone formation is visible in the trabecular bone, which is found in the upper and lower sites of the growth plate (Figure 2.12-II) and in the bone-implant interface (Figure 2.12-III). The bone condyle tissue (Figure 2.12-IV) can be used as positive control and spleen tissue (Figure 2.12-V) as negative control.

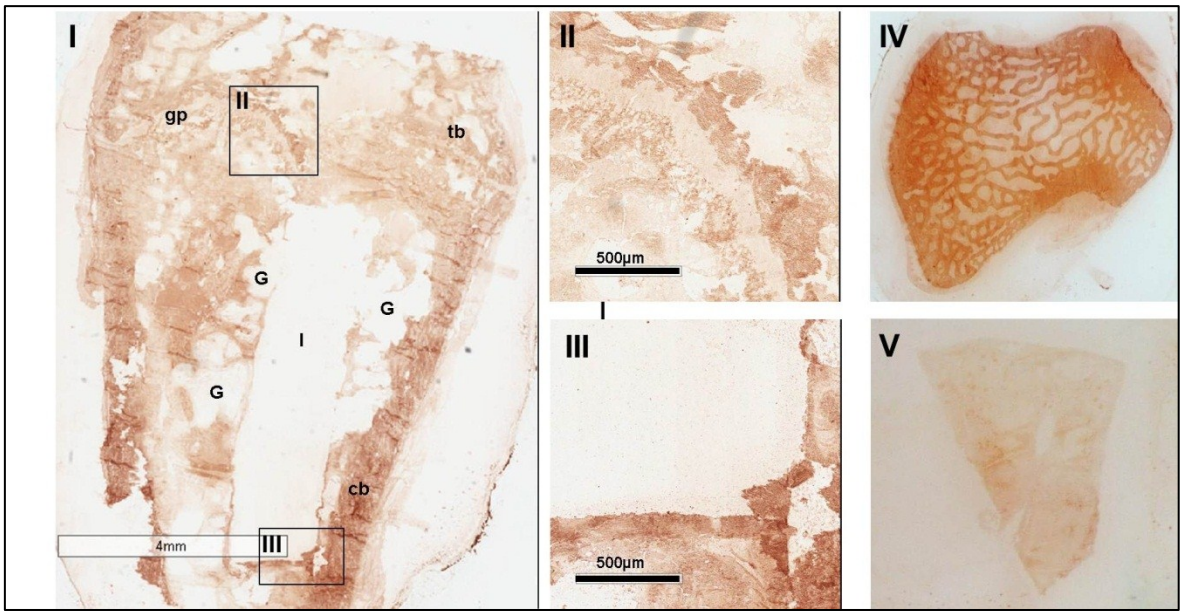

Figure 2.12: Collagen I antibody staining in bone tissue embedded in Technovit 9100 New (I). In higher magnification, the region of the growth plate (II) and the implant-bone interface (III) are visible. Condyle tissue (IV) has been used as positive control and spleen tissue (V) as the negative control. I: implant, G: gas formation, tb: trabecular bone, cb: cortical bone, gp: growth plate.

3 Part 2: *In vivo* degradation of binary Mg alloys – a long-term study

3.1 Aim of this part

In this study, pure Mg and the two binary alloy systems magnesium-silver (Mg-Ag) and magnesium-gadolinium (Mg-Gd) were chosen to minimize the influence of various alloying elements on the degradation performance of the implants. Consequently, possible changes in degradation behavior can be caused by one single alloying element. Pure Mg, Mg2Ag and Mg10Gd were selected in our study to investigate the performance of the alloy in the bone tissue concerning the degradation, the gas formation and the bone-implant interface up to 36 weeks.

The elements used are silver (Ag) and gadolinium (Gd). Ag has been shown to improve the mechanical properties and enhance the degradation resistances of Mg-Ag materials after suitable heat treatment. Furthermore, the Mg2Ag alloy appeared biocompatible in terms of cytotoxicity and cytocompatibility in *in vitro* cell tests and exhibited antibacterial properties in *in vitro* experiments (8).

The REEs are known to increase the mechanical properties and the corrosion resistance of the Mg alloys (19, 47, 48). More specifically, a study performed with various concentrations of Gd in Mg alloys (Mg5Gd, Mg10Gd and Mg15Gd) exhibited that a weight percentage of up to 10 % Gd can improve the degradation performance of the material, but a Gd concentration higher than 10 % cannot further enhance the degradation resistance (48). From a biological point of view, it is mentioned that REEs are used in anticancer drugs because of their anti-carcinogenic properties (49, 50).

Pure Mg, Mg2Ag and Mg10Gd alloys have been already used and studied in *in vitro* cell experiments. All three alloys showed promising results in cell viability tests (3, 35, 51).

The second part of this thesis was to investigate the degradation performance of pure Mg, Mg2Ag and Mg10Gd pins in an *in vivo* long-term study of 36 weeks. The main research question of this study was to investigate if there is a significant influence of Ag and Gd alloying elements on the degradation performance of these alloys in comparison to the pure Mg, in *in vivo* conditions.

3.2 Materials and Methods

3.2.1 Implants

3.2.1.1 Materials production

For this part of the thesis, three different Mg alloys were used: pure Mg, Mg2Ag and Mg10Gd. The materials were cast and prepared by Helmholtz-Zentrum (HZG), Geesthacht, Germany. For the casting, pure materials were used: Mg (99.99 %), Ag (99.99 %), Gd (99.95 %). The whole procedure of materials production was descripted in details by Myrissa et al. 2016 (3). The extrusion rods of pure Mg and Mg10Gd were reduced in diameter of 1.6 mm by the turning method (Ernst Wittner, GesmbH, Vienna, Austria) and the Mg2Ag by the wire drawing method. After the casting and extrusion steps, the cylindrical pins of pure Mg, Mg2Ag and Mg10Gd were sterilized by gamma radiation dose of 29.2 KGy (performed by the company BBF GmbH, Stuttgart, Germany).

The chemical composition and the contents of Ag and Gd were determinded by X-ray fluorescence spectrometer (Bruker AXS S4 Explorer, Bruker AXS GmbH., Germany) and are shown in Table 3.1.

Table 3.1: Chemical composition of pure Mg, Mg2Ag and Mg10Gd pins (3).

Alloy	Chemical composition wt. %					
	Ag	**Gd**	**Fe**	**Cu**	**Ni**	**Mg**
Pure Mg	-	-	0.0052	0.0023	0.0014	Bal.
Mg2Ag	1.75	-	0.002	0.0019	0.0013	Bal.
Mg10Gd	-	10.5	0.0029	0.0048	<0.0036	Bal.

3.2.2 Experimental design

For these experiments growing male Sprague–Dawley® rats 140-160 grams of weight and 5 weeks of age were used. These animals were divided into 4 different groups:

1) sham group (treated with a drill hole), (24 animals)

2) pure Mg-treated group (24 animals),

3) Mg2Ag-treated group (12 animals),

4) Mg10Gd-treated group (24 animals).

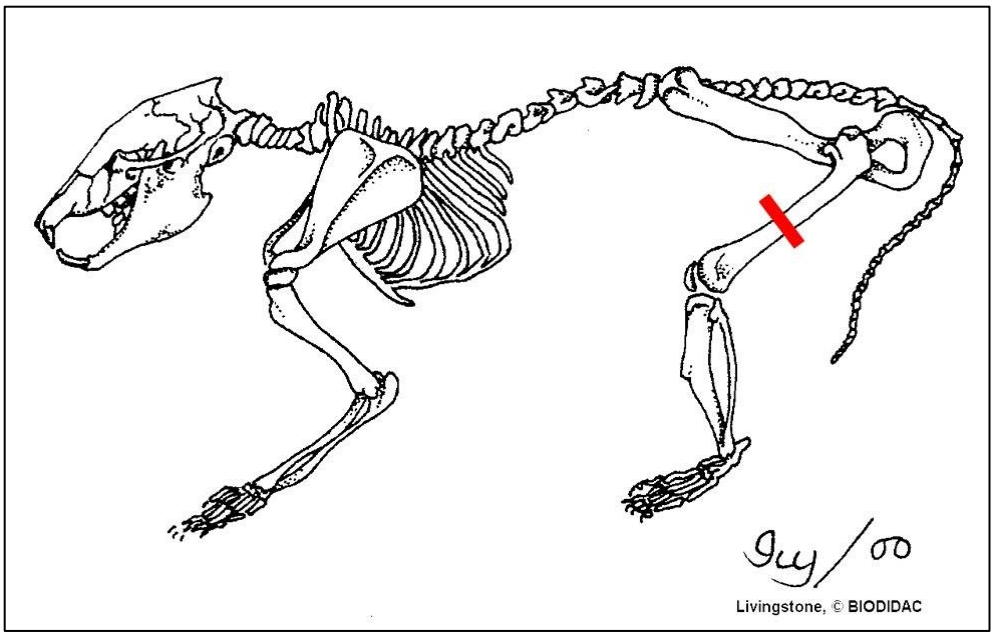

Figure 3.1: Transcortical animal model (1).

3.2.3 Ethical approval

All animal experiments were conducted under ethical respect for animals and were authorized by the Austrian Ministry of Science and Research (accreditation number BMWF-66.010/0070-II/3b/2011). Rats were housed in groups of three in clear plastic cages on standard bedding. Water and a standard pellet diet were given ad libidum. The animals were under daily observation of certified animal caretakers and veterinarians.

3.2.4 Surgical procedure

The surgery procedure was conducted under general anesthesia. Cylindrical pins (1.6 mm diameter and 8 mm length) of pure Mg, Mg2Ag, and Mg10Gd alloys were implanted transcortically into the middle diaphysis of both femoral bones. The implantation surgery took place under general anesthesia. The whole surgical procedure and the postoperative treatment protocol have been described in details (6).

The rats were allowed to move freely in their cages without external support and unrestricted weight bearing. The daily clinical observation was performed throughout the study period.

3.2.5 Micro-focused Computed Tomography *in vivo*

After the operation, micro-focused Computed Tomography (μCT) scans were performed with the Siemens Inveon micro-CT (Siemens AG, Healthcare Sector, Erlangen, Germany) at 5 different time points: 1, 4, 12, 24 and 36 weeks. During the μCT scans, the animals were anesthetized with volatile isoflurane (Forane®, Abbott AG, Baar, Switzerland). The μCT scan software used was the Siemens Inveon Acquisition Workplace 1.2.2.2 (Siemens Healthcare GmbH, Erlangen, Germany). Scans of the rats were performed at 70 kV voltage, 500 μA current, and 1000 ms exposure time. The effective pixel size was 35.04 μm.

Table 3.2: Number of the animals used per alloy per time point for the *in vivo* medium resolution µCT scans.

n=number of animals	Groups	Sham	Pure Mg	Mg2Ag	Mg10Gd
	Time				
n	**1w**	6	6	6	6
n	**4w**	6	6	6	6
n	**12w**	6	6	6	6
n	**24w**	6	6	6	6
n	**36w**	6	6	6	6

3.2.6 MIMICS evaluation

The µCT scans were reconstructed and, afterwards, data were converted into DICOM data. These DICOM data were used for the 3-D morphometric analysis and pin volume and surface as well as the gas volume calculated with the software Materialise Mimics® (Version 15.0 and 17.0, Materialise, Leuven, Belgium). Pin volume, pin surface and gas formation were segmented from the µCT data, following the measurement process fully described by Kraus et al. (6). The degradation rate (DR) [mm/year] of each alloy was also evaluated through pin volume and surface by the equation:

$DRi = \Delta xi / \Delta t$ with $\Delta xi = \Delta Vi / Si$,

where i is the observation time point, ΔVi is the change of the volume between the observation time point i-1 and I (Δt) in mm^3 and Si is the surface area at the

observation time point I in mm^2 (3, 7). For each time point, 6 bones (3 animals per time point) were used.

Table 3.3: Number of the animals which were used for pin volume and surface, gas volume and degradation rate evaluations of the different Mg alloys at different time points.

n=number of animals	groups	Pure Mg	Mg2Ag	Mg10Gd
	time			
n	1w	3	3	3
n	4w	3	3	3
n	12w	3	3	3
n	24w	3	3	3
n	36w	3	3	3

3.2.7 Micro-focused Computed Tomography *ex vivo*

After euthanization, the explanted bones were embedded in Technovit 9100 New 9100 New and scanned with a high resolution protocol which can exhibit more details regarding the degradation performance of the material during the bone healing process. These high resolution µCT scans were performed at 80 kV voltage, 500 µA current and 1050 ms exposure time. The effective pixel size was 18.93 µm.

Table 3.4: Number of the animals which were used per alloy per time point for the *ex vivo* high resolution µCT scans.

n=number of animals	groups	Pure Mg	Mg2Ag	Mg10Gd
	time			
n	4w	6	6	6
n	24w	6	3	6

3.2.8 Euthanasia

For general anesthesia, volatile isoflurane (Forane®, Abbott AG, Baar, Switzerland) was used. For euthanasia, 25 mg sodium thiopental (Thiopental® Sandoz, Sandoz GmbH, Kundl, Austria) was injected into the cardiac ventricle which led to immediate cardiac arrest (52). Animals were euthanized 4, 12, 24, 36 weeks after the implantation.

3.2.9 Histology

Technovit 9100 New embedding method

Four and twenty-four weeks (2 bones per alloy per time point) after the implantation, the bones were explanted and were scanned in µCT with a high resolution protocol. For histology, the Technovit 9100 New (Technovit 9100 New®, Heraeus Kulzer, Frankfurt, Germany) embedding method was used as fully described by E. Willbold and F. Witte (27). The whole procedure of Technovit 9100

New was already described in section 2.1.1. After the polymerisation and cutting, the sections were put in 37 ^{o}C for 2 days in order to get dried very well. The sections were stained with 0.1 % toluidine blue-O.

3.2.10 Statistical Analysis

Results were analyzed using IBM SPSS Statistics 22 (SPSS: Version 22.0. Armonk, NY, USA).

The results of pin volume, pin surface and gas volume between the three Mg alloys at each time point were analyzed by ANOVA one-way test. The significance level was set up on the p-value ($p < 0.05$, $p < 0.01$ and $p < 0.001$).

The results of the *in vivo* degradation rates were analyzed with the SPSS Mann-Whitney U test. The significance level was set up on the p value of 0.05.

3.3 Results

In this part of the thesis, the research question focused on how pure Mg, Mg2Ag and Mg10Gd cylindrical pins degrade after their implantation in Sprague-Dawley rats. This study was completed after 36 weeks.

In this study, 4 animal groups were used:

1) The sham group without an implant and only a drill hole was used to observe the normal healing process.
2) The pure Mg-treated group
3) The Mg2Ag-treated group and
4) The Mg10Gd-treated group.

Cylindrical pins were implanted in the femoral bones of growing male Sprague-Dawley® rats to compare the degradation performance of the different materials within the bone tissue during the healing process. *In vivo* µCT scans were performed, at 1, 4, 12, 24 and 36 weeks post-operative, with a medium resolution protocol. *Ex vivo* high resolution µCT scan images and corresponding histological bone tissue sections stained with toluidine blue-O were performed, at 4 and 24 weeks after the operation, in order to investigate the general bone morphology during the degradation process.

3.3.1 Micro-focused Computed Tomography (µCT)

The following results reveal the degradation performance and the reaction of surrounding bone tissue within the experimental groups of pure Mg, Mg2Ag and Mg10Gd in comparison to the sham group.

The image (Figure 3.2) shows the µCT scans of the sham, pure Mg, Mg2Ag and Mg10Gd animal groups performed at 1, 4, 12, 24 and 36 weeks. After µCT reconstruction, the 3D morphometric analysis through Mimics Software was performed. Pin volume and surface were calculated in order to evaluate the degradation rates of the implants.

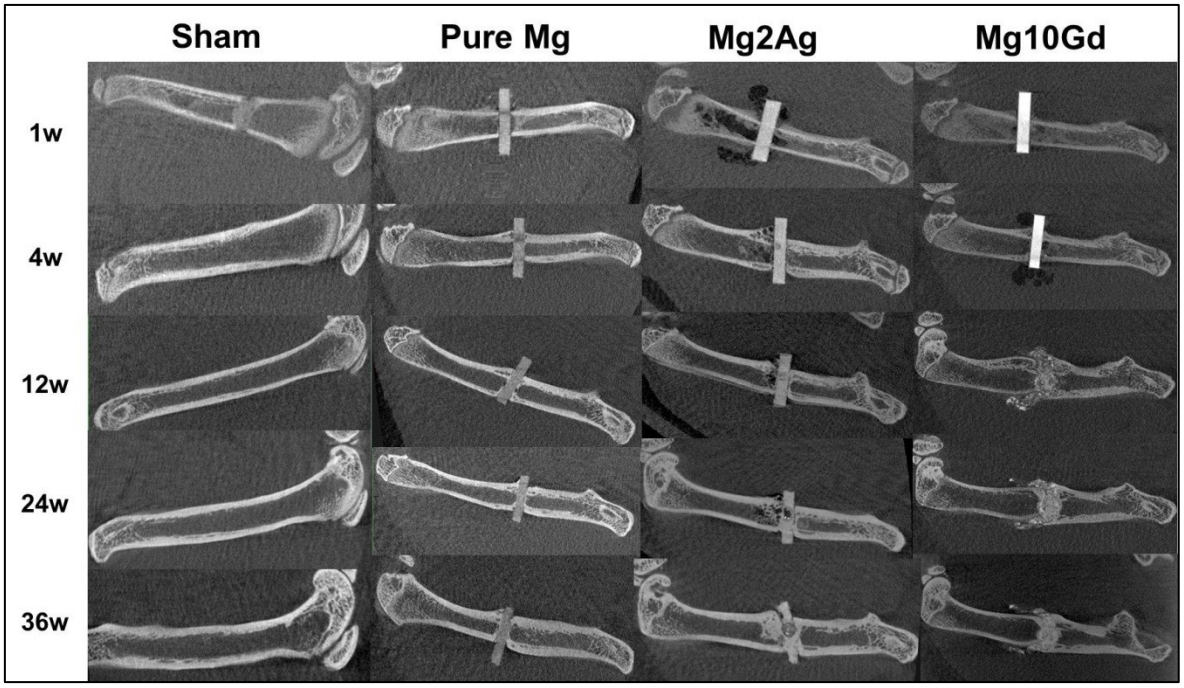

Figure 3.2: Sagittal 2-dimensional (2D) µCT scans revealing the normal bone healing process of the sham group, and the degradation performance of pure Mg, Mg2Ag and Mg10Gd materials at 1, 4, 12, 24 and 36 weeks after implantation in the femoral bones of growing Sprague-Dawley® rats (n = 6 animals/group) (2).

In the sham group, the drill hole was obvious the first week after the operation. The bone was totally healed at 4 weeks after the implantation (Figure 3.2, Sham group).

In the µCT images of the pure Mg pins, a low amount of gas formation was seen around the pins within the intramedullary cavity at the first week after the operation, whereas, no gas formation was observed 4, 12, 24 and 36 weeks after the implantation. Moreover, a close contact between the bone and pin surface has been observed 12 weeks after the implantation and consequently, new bone formation was visible around the implant at 12, 24 and 36 weeks post-operative (Figure 3.2, pure Mg group).

In the µCT images of the Mg2Ag pins, gas cavities within the intramedullary cavity and also in the surrounding tissue can be observed at the first week after the implantation. 4 weeks post-operative, gas was reduced and remained only within the medullary cavity around the implant. The amount of gas formation was further decreased at 12, 24 and 36 weeks post-operative. Since 12 weeks after the operation, bone attachment to the pin surface succeeded and, consequently, new bone formation was observed 12, 24 and 36 weeks after the operation. 12 weeks post-operative, a successful bone contact to the implant surface could be observed. This contact allowed the stable bone adherence and new bone formation around the pin surface which was obvious 24 and 36 weeks post operation (Figure 3.2, Mg2Ag group).

In the µCT images of Mg10Gd pins, a low amount of gas was exhibited 1 week after the implantation. 4 weeks post-operative, high amount of gas was observed especially in the surrounding tissue and first hints of degradation was visible. 12 weeks post-operative there was no gas formation. Moreover, 12, 24 and 36 weeks after the implantation, the pins were broken and disintegrated to small particles which were surrounded by new formed bone tissue (Figure 3.2, Mg10Gd group).

Table 3.5: Calculated pin volume, pin surface and gas volume of pure Mg pins with mean values (M) and standard deviation (SD), 1, 4, 12, 24 and 36 weeks after *in vivo* implantation.

Pure Mg						
	pin volume mm^3		pin surface mm^2		gas volume mm^3	
time	M	SD	M	SD	M	SD
1w	15.67	0.148	56.46	5.599	5.01	6.885
4w	15.24	0.102	57.26	3.983	0.02	0.204
12w	14.45	0.253	58.67	9.172	0.05	0.041
24w	13.15	0.323	57.93	2.835	0.12	0.178
36w	11.41	0.626	79.99	17.323	0.02	0.013

Table 3.6: Calculated pin volume, pin surface and gas volume of Mg2Ag pins with mean values (M) and standard deviation (SD), 1, 4, 12, 24 and 36 weeks after *in vivo* implantation.

Mg2Ag						
	pin volume mm^3		pin surface mm^2		gas volume mm^3	
time	M	SD	M	SD	M	SD
1w	15.87	0.118	47.87	1.034	20.04	14.303
4w	14.90	0.310	56.92	4.455	2.34	0.865
12w	13.49	0.282	71.04	6.571	2.65	1.211
24w	12.64	0.408	64.22	4.191	1.16	1.449
36w	11.62	0.876	74.86	7.601	1.01	0.856

Table 3.7: Calculated pin volume, pin surface and gas volume of Mg10Gd pins with mean values (M) and standard deviation (SD), 1, 4, 12, 24 and 36 weeks after *in vivo* implantation.

Mg10Gd						
	pin volume mm^3		pin surface mm^2		gas volume mm^3	
time	Mean	SD	Mean	SD	Mean	SD
1w	15.50	0.241	45.06	0.299	0.77	1.267
4w	14.00	0.741	48.77	3.499	80.26	117.699

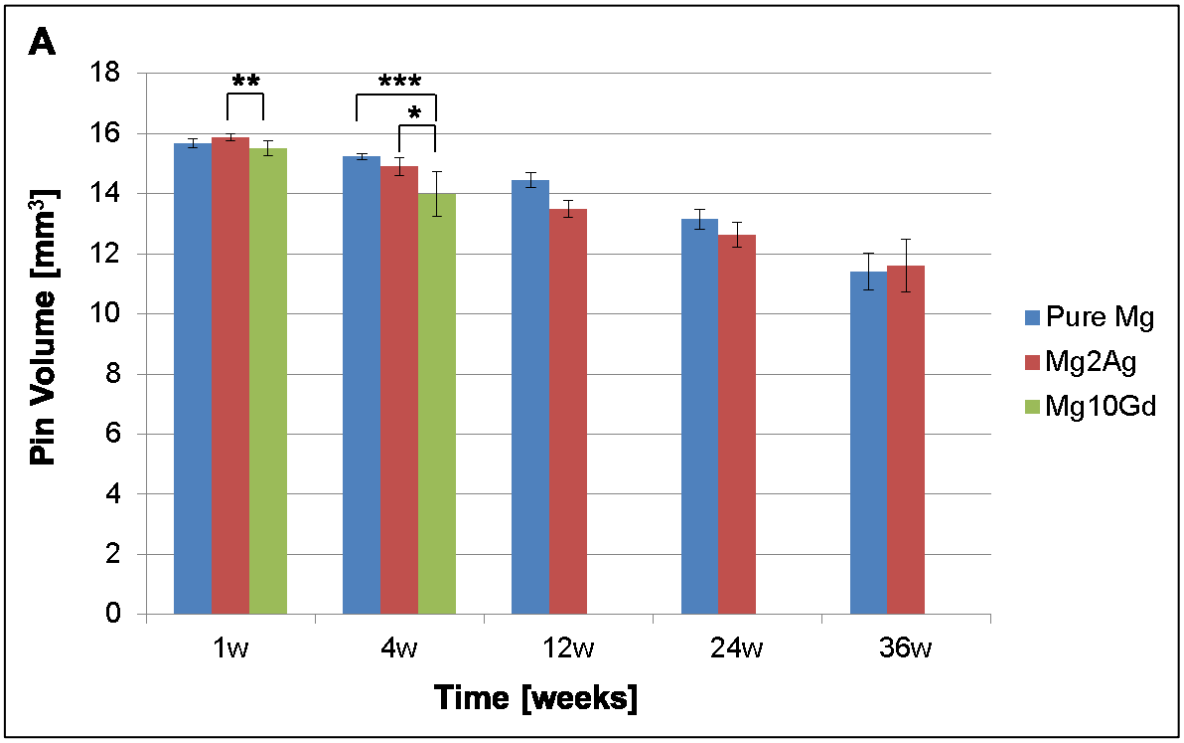

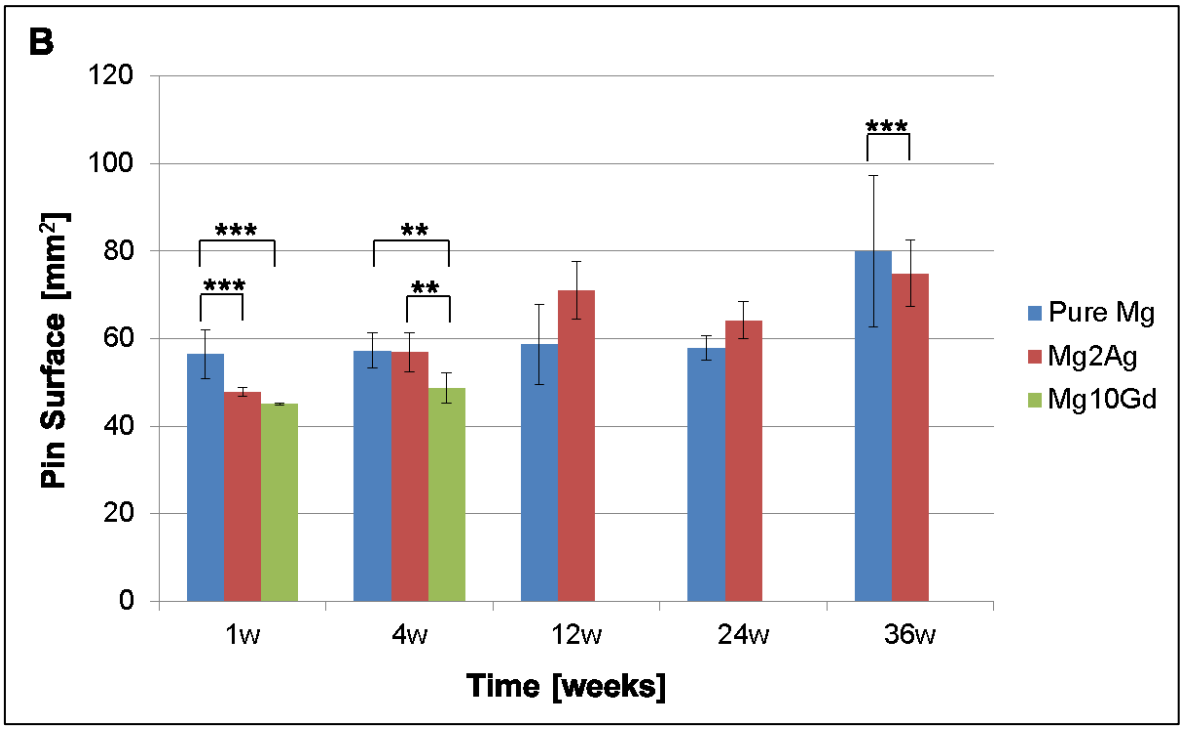

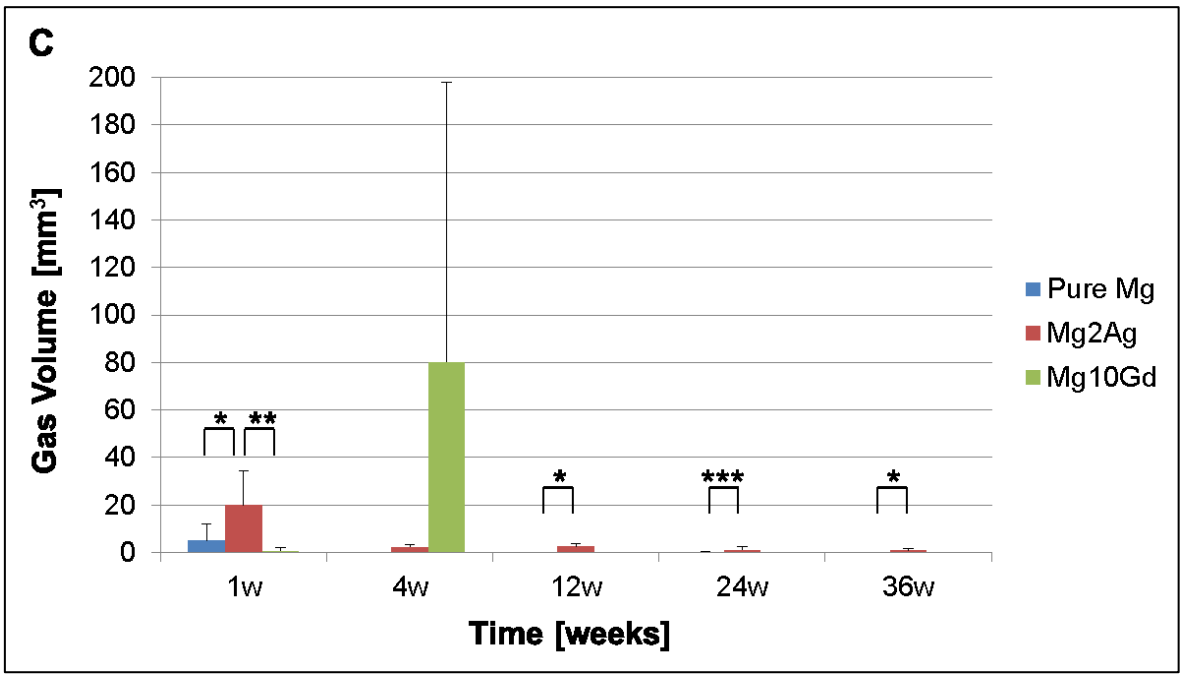

Figure 3.3: Pin volume (A), pin surface (B) and gas volume (C) evaluation of pure Mg, Mg2Ag and Mg10Gd pins 1, 4, 12, 24 and 36 weeks after the operation (n = 6 bones/alloy group). *, ** and *** indicate the significant difference of p-value $p<0.05$, 0.01 and 0.001, respectively (2).

The pin volume of the pure Mg was gradually reduced within the study of 36 weeks (Figure 3.3-A), whereas the pin surface remained stable (Figure 3.3-B). Moderate and linear pin volume loss and stable pin surface values indicated that pure Mg material displayed homogeneous and slow degradation during the long-term *in vivo* study. The gas evolution of pure Mg pins was the lowest compared to the gas evolution of Mg2Ag (gas evolution of pure Mg was significantly lower than the one of Mg2Ag) and Mg10Gd at first week after the implantation. Gas evolution was further decreased at 4, 12, 24 and 36 weeks (Figure 3.3-C). Pin volume and surface and gas volume evaluations were inconsistency with the μCT images results (Figure 3.2, pure Mg group).

The Mg2Ag pin volume was also gradually decreased during the long-term study of 36 weeks (Figure 3.3-A). The pin surface of Mg2Ag pins was augmented at the fourth week post-operative and remained at the same levels at 12, 24 and 36 weeks of the study (Figure 3.3-B). Mg2Ag exhibited the highest hydrogen evolution the first week, after the implantation, compared to pure Mg and Mg10Gd. 12, 24 and 36 weeks the gas production was decreased (Figure 3.3-C). The gas formation of Mg2Ag pins was significantly higher than the one of pure Mg pins 4 weeks after the operation, whereas, 12, 24 and 36 weeks post-operative, the gas evolution was significantly higher than the gas production of pure Mg. The above results were in accordance with the μCT images of the Mg2Ag alloy (Figure 3.2, Mg2Ag group).

The pin volume and surface and the gas volume of Mg10Gd pins were evaluated only for the first and fourth week post-operative. Mg10Gd pins lost their integrity after 12 weeks, and consequently, the pin volume and surface were not feasible to be calculated for the subsequent time points. The pin volume of Mg10Gd alloy was reduced 4 weeks after the implantation (Figure 3.3-A) and the pin surface maintained at the same level (Figure 3.3-B). The gas volume (Figure 3.3-C) was increased at 4 weeks compared to the first week after the operation. 12, 24 and 36 weeks after the implantation, there was no gas evolution which was in correspondence with the μCT results of Mg10Gd alloy (Figure 3.2, Mg10Gd group).

3.3.2 Calculation of the degradation rates

Degradation rates of pure Mg, Mg2Ag and Mg10Gd pins were calculated through the pin volume and pin surface values and are shown in Table 3.8 and in Figure 3.4.

Table 3.8: Calculated degradation rates [mm/year] with mean values (M) and standard deviation (SD) of the pure Mg, Mg2Ag and Mg10Gd pins at different time points during the long-term *in vivo* study.

	Pure Mg		**Mg2Ag**		**Mg10Gd**	
	Mean	**SD**	**Mean**	**SD**	**Mean**	**SD**
1w	0.38	0.124	0.24	0.13	0.67	0.284
4w	0.13	0.065	0.29	0.10	0.53	0.213
12w	0.09	0.038	0.13	0.061		
24w	0.098	0.036	0.058	0.034		
36w	0.097	0.038	0.021	0.017		

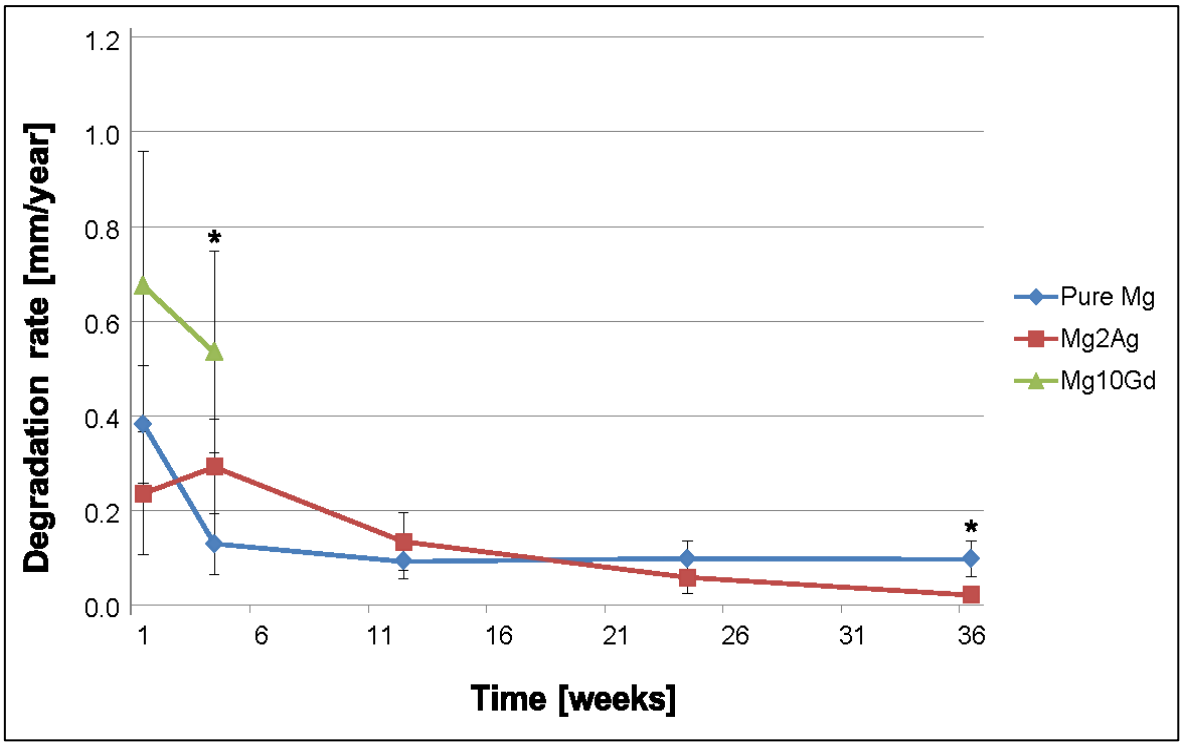

Figure 3.4: Degradation rates of pure Mg, Mg2Ag and Mg10Gd pins in a long-term *in vivo* study at 1, 4, 12, 24 and 36 weeks after the operation (n = 6 bones/alloy group). * indicates the significant difference of p-value $p<0.05$, between the 3 different Mg materials at each time point (2).

The initial degradation rate of pure Mg was 0.38 ± 0.12 mm/year 1 week after the operation and was reduced to 0.13 ± 0.06 mm/year 4 weeks after the implantation. Additionally, the degradation rate remained stable till the termination of the study (0.1 ± 0.04 mm/year) (Figure 3.4). These results revealed a slow and moderate degradation behavior of pure Mg implants.

The Mg2Ag degradation rate started with 0.24 ± 0.13 mm/year. 4 weeks post-operative, the degradation rate increased moderately, but not significantly. The degradation velocity of Mg2Ag pins remained stable until the twelfth week after the implantation but it was gradually reduced at twenty-fourth and thirty-sixth (final value: 0.02 ± 0.017 mm/year) week post-operative. The degradation performance of Mg2Ag alloy was moderate and slow within the long-term study of 36 weeks (Figure 3.4).

On the contrary, the degradation velocity of Mg10Gd started at 0.67 ± 0.28 mm/year 1 week after the implantation and was decreased to 0.53 ± 0.21 mm/year 4 weeks post-operative. The degradation rate of Mg10Gd was the highest compared to the degradation rates of pure Mg and Mg2Ag at 4 weeks after the operation (Figure 3.4). Mg10Gd pins lost their integrity after 12 weeks, and consequently, the pin volume and surface and, as a result, the degradation rates were not feasible to be calculated for the subsequent time points.

3.3.3 Bone implant interaction

Beside the *in vivo* medium resolution µCT scans, *ex vivo* high resolution µCT scans as well as histological bone tissue sections embedded in Technovit 9100 New and stained with toluidine blue-O were used to investigate the general bone morphology during the degradation procedure. The *ex vivo* high resolution µCT scans of the embedded samples were compared with the equivalent histological sections (Figure 3.5).

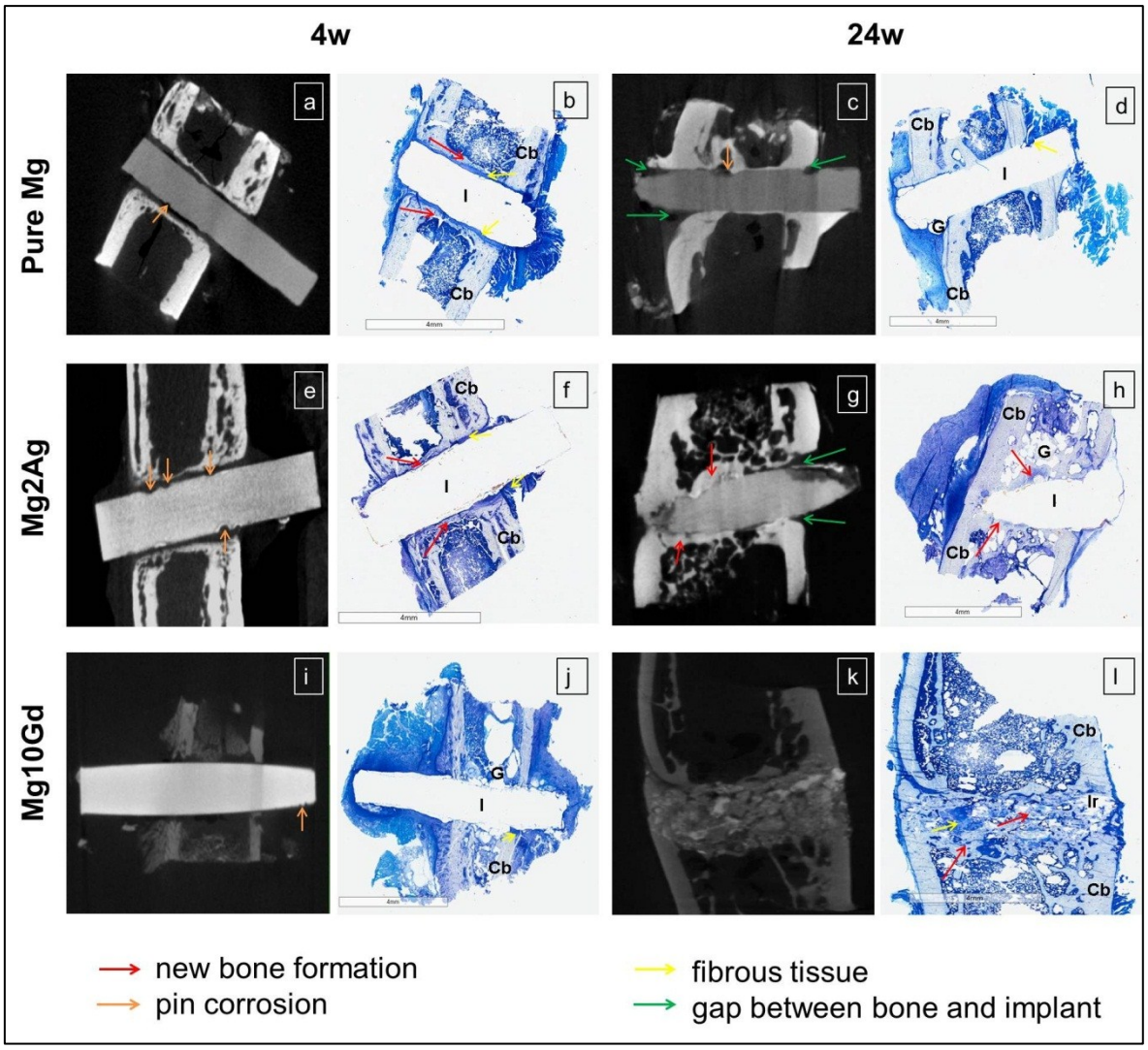

Figure 3.5: *Ex vivo* high resolution µCT reconstructed images (2D) of explanted pure Mg-, Mg2Ag- and Mg10Gd-treated femoral bones 4 and 24 weeks after the operation. The general bone morphology of these samples is shown in corresponding bone sections stained with Toluidine Blue-O. I: implant, Ir: implant remnants, Cb: cortical bone, G: gas bubbles, orange arrows: pin corrosion, yellow arrows: fibrous tissue, red arrows: new bone, green arrows: the gap between bone and implant (2).

The *ex vivo* high resolution µCT images of explanted bones treated with pure Mg (Figures 3.5-a and c), Mg2Ag (Figures 3.5-e and g) and Mg10Gd (Figures 3.5-i and k) displayed the degradation behavior of these alloys at 4 and 24 weeks post-

operative. The same scanned blocks were cut in thin slices and used for Toluidine blue-O staining.

Femoral bone with implanted pure Mg has shown no visible gas formation 4 weeks after the operation. In the high resolution scans (Figures 3.5-a, orange arrow), the first corrosion pits on the surface of the pin were observed. Moreover, fibrous tissue and new bone encapsulated the implants at this time point (Figures 3.5-a and b). Small gas cavities were noticeable within the medullary cavity at 24 weeks post-operative and a thin layer of bone surrounded the pins. Furthermore, a gap between the implant surface and bone was obvious (Figure 3.5-c; green arrows).

The Mg2Ag pin implanted into the femoral bone did not exhibit gas cavities 4 weeks after the operation. Moreover, first corrosion pits on the pin surfaces which are adjoined the intramedullary cavity were detected (Figure 3.5-e, orange arrows). At this time point, fibrous tissue and new bone surrounded the pin are visible (Figure 3.5-f). Small gas cavities were observed within the medullary cavity (Figure 3.5-h) and a gap between the bone and the implant surface was visible (Figure 3.5-g, green arrows) at 24 weeks after the implantation.

Small gas cavities within the intramedullary cavity around the pin were visible at the Mg10Gd implanted femoral bone 4 weeks post-operative (Figure 3.5-j). In addition, the first pin degradation was observed, especially on the site of the pin exposed to the surrounding tissue (Figure 3.5-i, orange arrow). Parts of the disintegrated implant were detected in cranial and caudal cortical bones and within the medullary cavity 24 weeks after the implantation (Figures 3.5-k and l). Furthermore, fibrous and especially bone tissue enclosed the material remnants (Figure 3.5-l).

4 Part 3: Elemental distribution of a REE-containing Mg alloy

4.1 Aim of this part

REE are used as alloying elements because they enhance the mechanical properties of the Mg alloy materials (19). The REE which have been already used as alloying elements and have been investigated for their promising enhanced degradation resistance of the Mg alloys are yttrium (Y), neodymium (Nd), cerium (Ce), Gd and lanthanum (La) (19, 48, 53).

In general, it is reported that REE can have toxic effects and can cause various negative health effects in mammals (54). A review study performed by Pagano et al. summarized the conclusions of different animal studies concerning the toxicity of REEs such as, Ce, Dysprosium (Dy), Gd, La, Nd and Y (55).

There are *in vitro* studies concerning the cytotoxicity of few Mg-REE alloys (34-36, 38, 42, 56). However, the *in vivo* experiments on the materials' toxicities which have been performed (6, 12, 40-42) are limited only to the effects of REE on the biological tissues that are close to the implant, but possible systemic effects have not been published yet (44). This kind of studies could be essential for novel materials.

In this thesis, Gd was used as alloying element. In general, it is known that Gd is toxic when it is present as free ion, but however, has very low toxicity to mammals when it is chelated (54). Gd-chelates can inhibit the Gd ion release (57). As a result, the chelator protects the various tissues from the free Gd ions and subsequently it causes rapid renal excretion of the Gd ions. Consequently, Gd accumulation in the body is diminished (58).

Gd complexes can be used in clinical applications as contrast agents in magnetic resonance imaging (MRI) (59). Nevertheless, it has been reported that Gd complexes can cause nephrogenic systemic fibrosis in patients with chronic kidney failure (60). Additionally, it has been mentioned that Gd can accumulate in the human body after administration of Gd-containing MRI contrast agents (GBCAs) (61, 62). Moreover, it has been referred that Gd accumulates in the organs of animals and humans such as in the bone (63), in the liver (64), in the brain (65) after administration of Gd-containing MRI contrast agents. However, the consequences of Gd accumulation in the human body are still unknown (61).

The last years, studies have been evaluating the promising anticancer properties of REE (66). More specifically, studies have been performed focusing on the promising antiproliferative and anticancer properties of Gd(III) as a binding ligand in various chemical complexes (67-73).

Although there are systemic toxicological studies concerning the Gd salts or Gd-chelated complexes there is still no information about the systemic effects of Mg-Gd biodegradable alloy into the animal body after its implantation.

The main aim of this study was to investigate the distribution of the Gd element in male growing Sprague-Dawley rats during the long-term *in vivo* study of 36 weeks. The main research question of this study was to investigate if there is an accumulation of the Gd element in different organs during the degradation of Mg10Gd alloy. For this purpose, the concentrations of Mg and Gd elements were analyzed, in different organs (brain, heart, kidney, liver, lung, muscle, spleen) and blood serum samples of rats treated with Mg10Gd biodegradable implant, at different time points.

4.2 Materials and Methods

4.2.1 Blood serum sampling

Blood was collected from sham and Mg10Gd-treated animal groups (n=6 animals/ group/ time point) at different time points after the operation (1, 4, 12, 24 and 36 weeks). Animals were under anesthesia with volatile isoflurane (Forane®, Abbott AG, Baar, Switzerland). The blood was collected from the tongual vein of the animals (Vena lingualis) (52). Lithium-Heparin tubes (S-Monovette®, Sarstedt AG & Co, Nümbrecht, Germany) and Heparin solution (Heparin, Biochrome Gmbh, Berlin, Germany) were used in blood collection. One ml of blood was collected in the tubes and 250 U/ml Heparin was added in order to decrease the possibility of blood coagulation. Then, the blood was centrifuged at 5000 rpm for 10 min at 4 ^{o}C. Afterrwards, the serum was collected in Eppendorf tubes and frozen immediately at -80 ^{o}C.

4.2.2 Organ sampling

After euthanasia (6 animals per time point per group), the body weight of each animal was measured. The femoral bones were explanted immediately after euthanasia and were kept at -80 °C. Additionally, the organs (muscle, lungs, heart, liver, spleen, kidneys and brain) of each animal were collected, weight measured and immediately frozen at -80 ^{o}C.

4.2.3 Determination of Mg and Gd concentrations in organs and blood serum samples

Organs samples and blood serum samples' analysis experiments were performed by Simone Bräuer (Department of Chemistry, Karl-Franzens University of Graz, Department of Chemistry). The concentrations of Mg and Gd elements were determined at 4, 12, 24 and 36 weeks post-operative with inductively coupled plasma triple quadrupole mass spectrometry (ICPQQQMS).

4.2.4 Statistical Analysis

Results were analyzed using IBM SPSS Statistics 22 (SPSS: Version 22.0. Armonk, NY, USA).

Statistical evaluation of the Mg and Gd concentrations were performed with the student t-test or one-way ANOVA.

4.3 Results

As the question whether the REE can be safely used as alloying elements on Mg biodegradable materials is still missing, this part of the study focused on the element's distribution of the Mg10Gd (a REE-containing Mg alloy) within the rat organs. The Mg and Gd element concentrations in organs and in blood serum samples of the sham the Mg10Gd-treated animal groups were investigated in order to deduce some additional conclusions about the accumulation and distribution pattern especially of the Gd element, which belongs to REE.

4.3.1 Mg and Gd concentrations in organ samples

The results showed that the muscle samples had the highest Mg concentrations whereas the lung samples had the lowest ones in both animal groups (Figures 4.1-A and B). The statistical analysis of these results showed that:

a) at each organ, between the sham and the Mg10Gd treated animal groups, there was no significant change in their Mg concentrations (t-test, $p>0.05$),

b) at each organ, between the different time points, there was also no significant difference (one-way ANOVA, $p>0.05$).

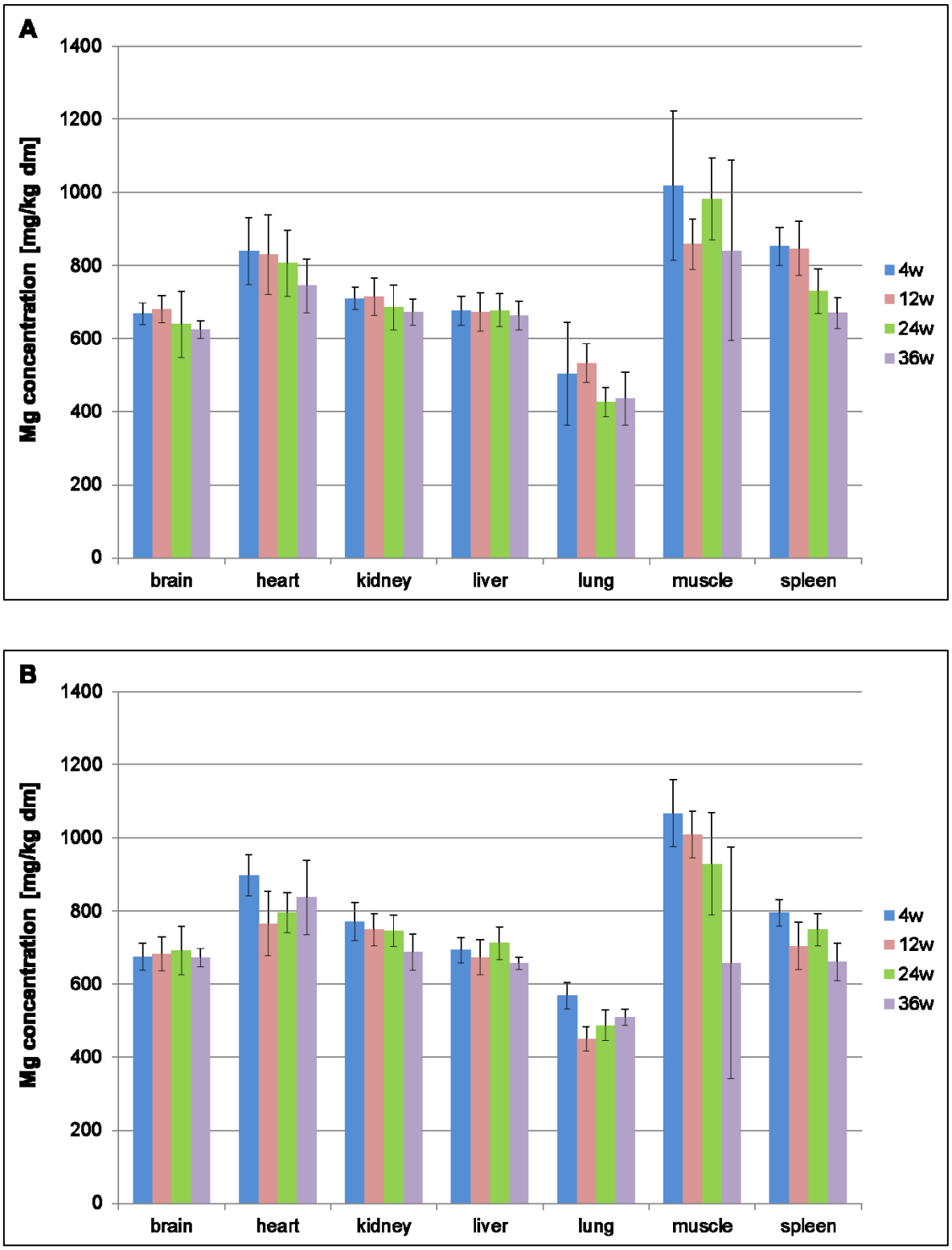

Figure 4.1: Mg concentrations of the organ samples of (A) sham and (B) Mg10Gd-treated animal groups at 4, 12, 24 and 36 weeks post-operative (n = 6 animals/group/time point).

The results of the Gd concentrations in the rat organs of sham and Mg10Gd-treated animal groups are shown in Figure 4.2.

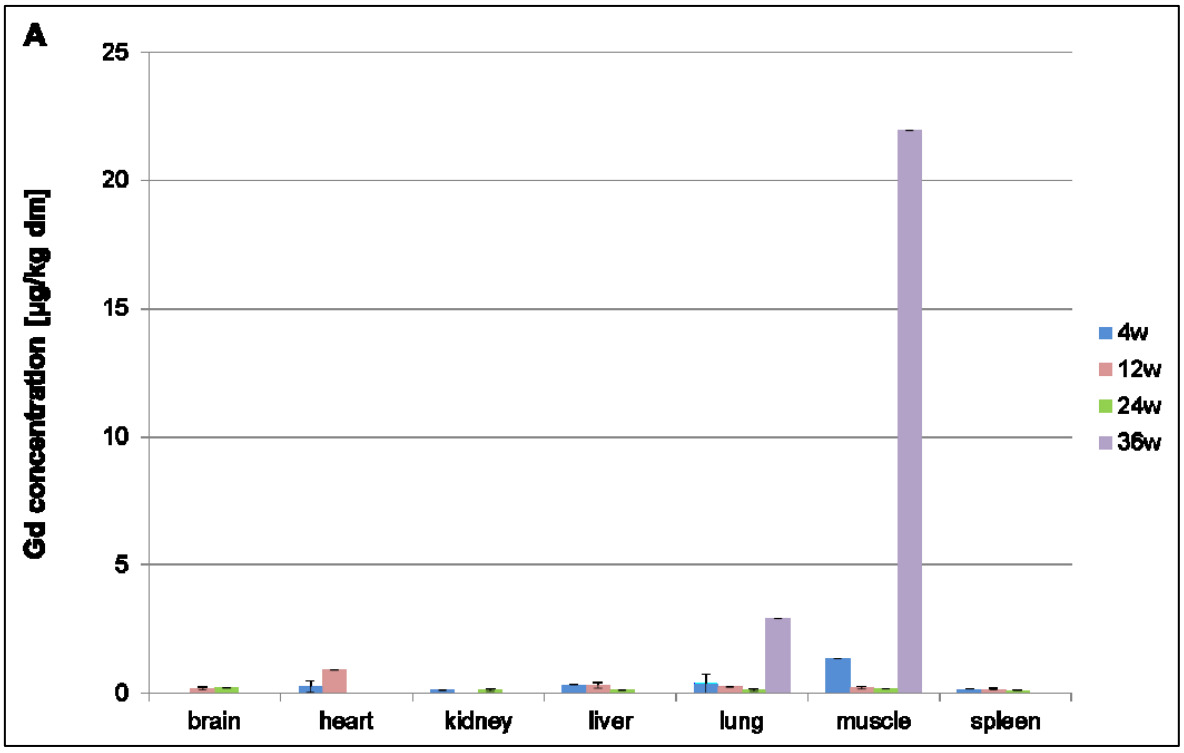

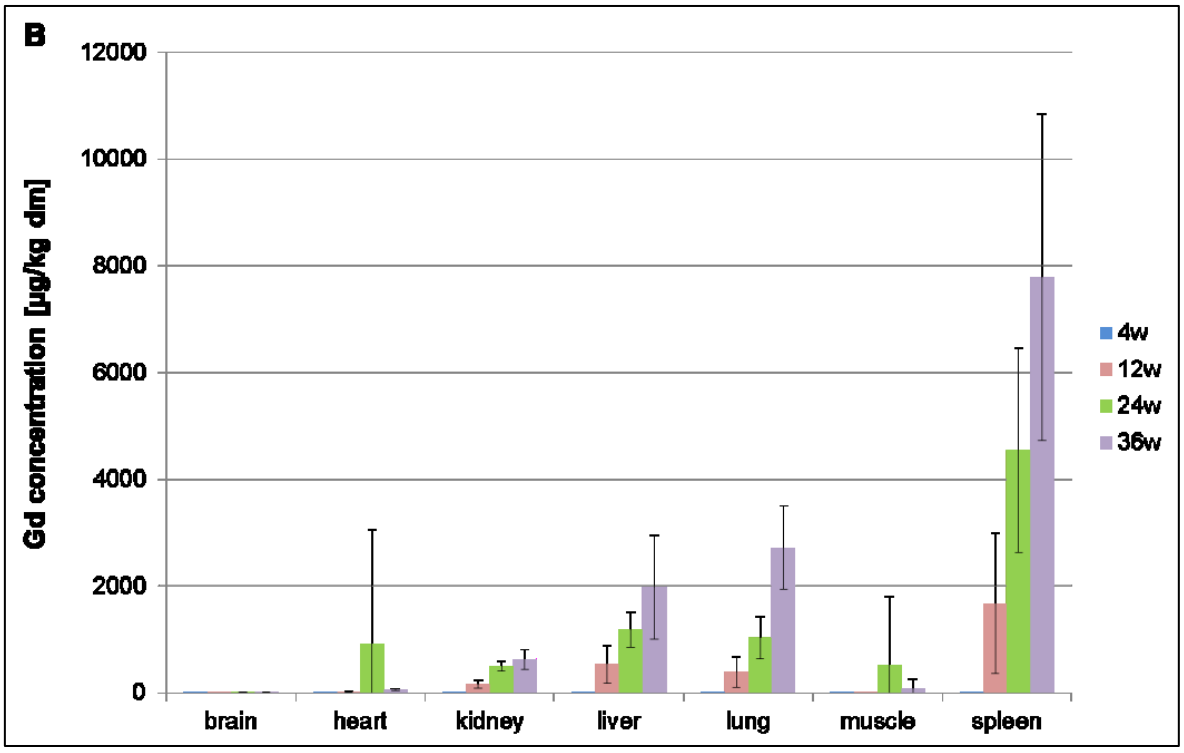

Figure 4.2: Gd concentrations of the organ samples of (A) sham and (B) Mg10Gd-treated animal groups at 4, 12, 24 and 36 weeks post-operative (n = 6 animals/group/time point).

The results showed that Gd concentration of the Mg10Gd-treated animal group was gradually increased in all organ samples and especially in kidney, liver, lung and spleen tissue during the 36 weeks' study (Figure 4.2-B). On the contrary, the values of Gd concentration in the organs of the sham animal group were very low (Figure 4.2-A).

The statistical analysis of these results showed that:

a) at each organ, between the sham and the Mg10Gd treated animal groups, there was significant change in their Gd concentrations (t-test, $p<0.05$), and specifically the Gd concentrations of Mg10Gd-treated animal groups were significantly higher than the ones of the sham group

b) at each organ, between the different time points, there was a significant increase of Gd concentration (one-way ANOVA, $p<0.05$) on Mg10Gd-treated animal group.

4.3.2 Mg and Gd concentrations in serum samples

No significant difference could be observed between the Mg concentrations in the different groups (t-test, $p>0.05$), (Figure 4.3-A). No significant change could be observed between the Gd concentrations in the different groups (Figure 4.3-B).

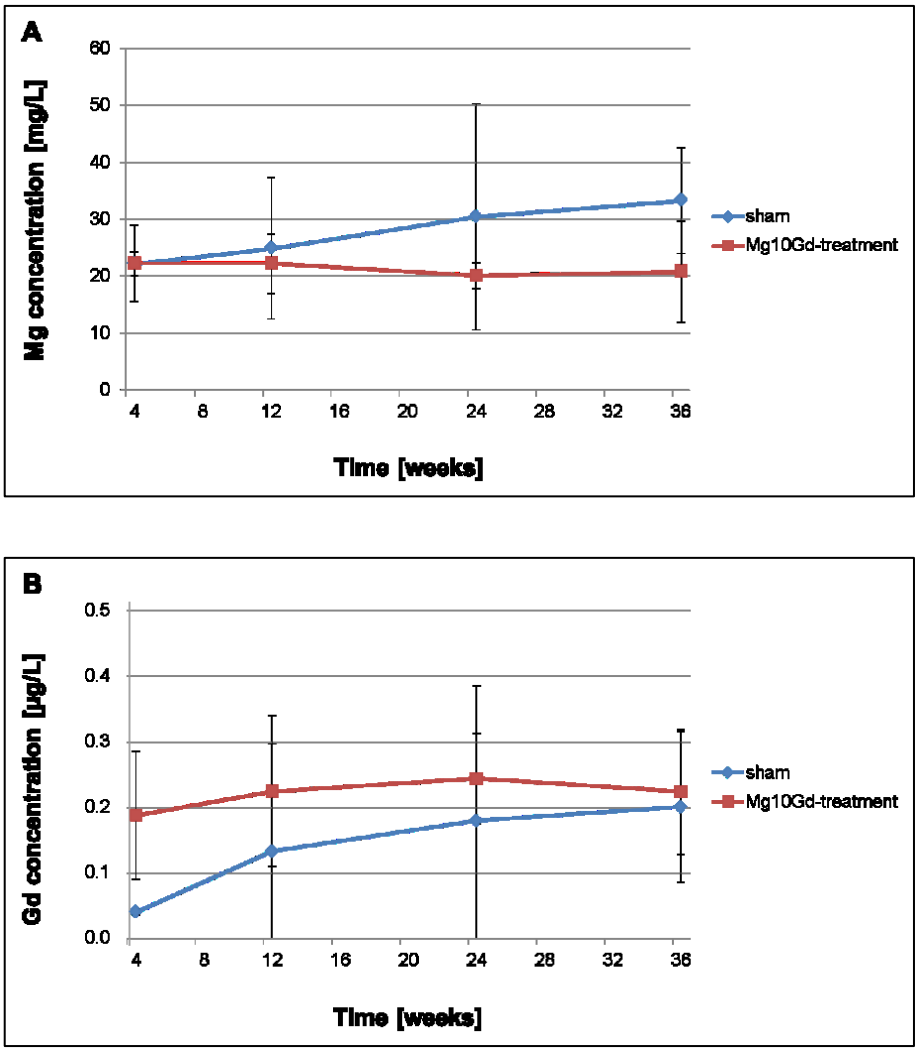

Figure 4.3: Mg (A) and Gd (B) concentrations of the blood serum samples of sham and Mg10Gd-treated animal groups at 4, 12, 24 and 36 weeks post-operative (n = 6-12 blood serum samples/animal group/time point).

5 DISCUSSION

5.1 Part 1: Establishment of the Immunohistochemistry in Technovit 9100 New

The first aim of this study was to establish the Technovit 9100 New in rat bone tissue. For this purpose, distal epiphysis bone tissues which were implanted with bioresorbable Mg alloys were used. Different kind of general stainings and immunostainings were employed. Few of them were also used in bone tissues embedded in paraffin.

Paraffin and Technovit 9100 New are two different embedding methods. Their application depends on the tissue samples used in the specific study and the research question you want to answer.

Paraffin embedding

Paraffin embedding method is widely used for the histology of soft tissues. Hard tissues such as bone and teeth need to be decalcified before their embedding in paraffin but during these decalcification steps, the molecules of the tissue can be destroyed or their molecular and chemical structure can be changed. This can result in losing of crucial epitopes. Finding the proper decalcification solution and incubation time of the sample on the decalcification solution are important steps. On one hand, over-decalcification can cause loss of the nuclear staining and impair the staining (74). On the other hand, less-decalcification can maintain the hardness of the bone tissue and cracks could occur during the cutting process. In addition, paraffin embedding method could not be used in our experiments because of the bone samples which are implanted with Mg alloys pins. Generally, paraffin embedding method is not suitable for bones or teeth samples which are implanted with hard materials such as titanium, steel or Mg and Mg alloys. A possible implant removal from the tissue, before its embedding in paraffin, could cause loss of the formed bone around the implant surface and consequently crucial information regarding the bone-implant interface could be lost. Nevertheless, paraffin embedding method is commonly used during the last

decades and consequently, there are a plenty of conventional stainings as well as commercial antibodies which can be used and work properly. Additionally, plenty of information and staining procedures are available in the literature.

Technovit 9100 New embedding

Technovit 9100 New is a method that can be used for the embedding of hard tissues such as bone and teeth which are implanted with Mg alloys or biodegradable polylactide/polyglycolide-based implants (27). No decalcification steps, as well as implant removal, have to be performed before the embedding. As a result, a better preservation of the epitopes and the tissue morphology can be succeeded and consequently a possibly closer to the real *in vivo* conditions observation could be achieved (45). However, the Technovit 9100 New embedding procedure and especially the cutting procedure need specific equipment, such as a rotation microtome with a hard-cutting knife. Moreover, there is only less information about the proper working protocols of the conventional stainings and immunostainings in rat bone tissues which are embedded in Technovit 9100 New. For this reason, there is still a necessity of testing Technovit 9100 New efficiency on different markers in order to adapt to the standard protocols and obtain the best quality of the stainings, which could be really time-consuming.

Stainings performed in bone samples embedded in Technovit 9100 New and in paraffin

Toluidine Blue-O staining belongs to general stainings and can be used for indicating the morphology of the bone tissue. It is used for detecting old and new bone, the osteoid, osteoblasts and osteocytes. Hematoxylin-Eosin is also a general staining which is widespread used in medical research. In bone tissue, HE

can also show the general overview of the bone morphology. It exhibits the growth plate, the trabecular and cortical bone, the bone marrow cells and the granulocytes in the areas with accumulated cells. It gives a general overview of the cells and shows the cellular organization in the bone tissue. For example, in higher magnification, the five zones (rest zone, proliferation zone, hypertrophic zone, calcified zone and ossification zone) of the growth plate are visible. Collagen II can be found in cartilage and growth plate region of the bones. Osteoblasts, which play a key role in the new bone formation process, can be detected by osteocalcin antibody.

All the mentioned stainings worked properly at both paraffin and Technovit 9100 New embedding methods. Regarding the general stainings of the toluidine blue-O and HE, it could be observed that the colors of the paraffin embedded bone tissues are paler than these of the Technovit 9100 New embedding bone tissues. A possible explanation could be the decalcification of the bone which destroys the original morphology of the bone. Moreover, the incubation times of the paraffin embedding bone tissues in the staining solutions are shorter compared to these for the Technovit 9100 New. This can be explained by the higher penetration capacity of each staining in paraffin embedded tissues due to the performed decalcification steps. The anti-collagen II and anti-osteocalcin antibodies showed similar results at both Technovit 9100 New and paraffin embedded rat bone sections.

Stainings performed in bone samples embedded in Technovit 9100 New

Safranin-O can detect the cartilaginous regions of the bone tissue (Figure 3.6). Movat's Pentachrom (Figure 3.7) is a staining that can be used for general bone morphology. It can be used for the detection of the growth plate, mineralised and non-mineralised cartilage, mineralised bone and non-mineralised bone (osteoid) which are stained in different colors. As a result, much information regarding the

general bone morphology could be provided by using this staining. On the other hand, the high diversity of colors of this staining can be a drawback because the interpretation of the results could be misleading or not properly performed. TRAP and Chloroacetate esterase stainings belong to the enzyme-based histochemical stainings. These stainings show the histo-topographical pattern of specific enzyme activities. The bone mass is controlled by the balanced activities of osteoblasts (new bone formation) and osteoclasts (bone resorption). TRAP is a staining which is used for detecting the presence of osteoclasts in bone tissue (27). Osteoclasts play an important role in the normal bone turnover process and in the remodeling process. Chloracetatesterase is a simple staining to detect the neutrophil granulocytes which play a key role in inflammatory reactions. Collagen I is the main component of bone, detecting the cortical and trabecular bone.

The preservation of the bone tissue morphology in Technovit 9100 New can be kept in a good quality. The Technovit 9100 New can be proved as a crucial methodology in the bioresorbable biomaterials field. Further studies in rat bone tissues have to be performed in order to have more available immunostaining markers' protocols and consequently obtain more information about the molecular mechanisms of bone healing process during the degradation of Mg alloys.

5.2 Part 2: *In vivo* degradation of binary Mg alloys – a long-term study

In this long-term study, two binary Mg alloying systems, Mg2Ag and Mg10Gd, were studied and compared to pure Mg.

The results of this long-term animal study indicated that Ag as well as Gd can affect the degradation rate and can influence the degradation performance of the Mg materials when they are added as alloying elements in a binary Mg system. A comparison between the degradation performances of pure Mg, Mg2Ag and Mg10Gd showed that pure Mg and Mg2Ag exhibited gradual pin volume reduction and low degradation rates within the study of the 36 weeks. These results indicated that pure Mg and Mg2Ag are slow degradable alloys degrading moderate and homogeneously. On the contrary, the Mg10Gd exhibited a high degradation rate at first and fourth week after the operation and an uncontrolled disintegration of the pins. The evaluation of the pin volume, pin surface and subsequently the degradation rate of the Mg10Gd material, 12, 24 and 36 weeks post-operative, were not feasible due to its disintegration into small particles.

The homogeneous and slow degradation behavior of pure Mg has been shown in other studies with different purity levels of the pure Mg (2, 3, 75, 76). It is reported that the reduction of impurities to very low amounts diminishes the degradation rate and displays a slower and homogeneous degradation especially in the first phase after implantation (75, 77). A study performed by Hofstetter et al. in which extreme high pure Mg samples (< 10 ppm impurity levels) were produced, showed a degradation rate of 0.010 ± 0.003 mm/year in *in vitro* conditions and 0.013 ± 0.003 mm/year in *in vivo* implantations (75). Compared to this study, the used pure Mg in the study of Tie et al., (76) exhibited initial corrosion rates at approximately 0.9 mm/year and decreased to 0.6 mm/year at 16 weeks post-operative (76). The initial degradation rate of 0.38 ± 0.12 mm/year and the final degradation rate of 0.1 ± 0.04 mm/year 36 weeks post-operative as well as the impurities up to 0.0089 wt% (3) are within the range of the degradation rates and impurity levels of these published studies.

In this study, the degradation performance of Mg2Ag was displayed to be more homogeneous and moderate because the degradation rate remained stable within the 36 weeks of the study. The slow degradation of Mg2Ag in the transcortical animal model provides the bone enough time for bone adherence at the implant and new bone formation around the pin's surface. As a result, the Mg2Ag pins were well-integrated into the femoral bone since 12 weeks post-operative and consequently bone remodeling process occurs simultaneously with the pin degradation process. Additionally, no adverse reactions on the normal bone healing process could be observed. The slow degradation of Mg2Ag alloy, seen in these results, is contradictory to the results of a study performed by Jähn et al. (21). At this study, two mice animal models, a non-fractured femoral bone and a fractured femoral bone, were used. The Mg2Ag nails were implanted into the intramedullary cavity of the femoral bones and an almost complete degradation of Mg2Ag nails before 210 days (30 weeks) was observed in the non-fractured animal model and 133 days (19 weeks) in the fractured one (21).

Both, pure Mg and Mg2Ag, showed slow degradation performance and good integration into the femoral bone after 36 weeks. The low amount of gas formation and as a result, the slow degradation of these materials, caused no additional adverse reactions to the normal bone healing process. The moderate degradation of these two materials allows a bone attachment to the implant surface and the bone formation around the implant surface especially at the part of the pin which is within the medullary cavity. On the contrary, Mg10Gd alloy disintegrates into smaller particles which remained visible until the end of the study.

This difference of the degradation performance rate of the Mg10Gd alloy could be possibly explained by its microstructure and the intermediate particle distribution. The microstructure analysis of the Mg10Gd pins exhibited Gd-rich intermetallic particles in the microstructure of the samples (3). These Gd-rich particles could be GdH_2 and Mg_5Gd which can be nobler than the Mg matrix and can cause a galvanic effect between the matrix and the particles (78). Consequently, a localized corrosion could occur which can possibly lead to the breakage and the fast disintegration of the Mg10Gd pins. This could be a reason why the in vivo degradation performance of Mg10Gd is not homogeneous till the end of the long-

term *in vivo* study. On the contrary, in the pure Mg and Mg2Ag pin samples which revealed a more homogeneous and moderate degradation performance, no particles were found (3).

The biological response of Mg10Gd alloy was studied by a high resolution μCT scan protocol and the corresponding histological bone sections. The *ex vivo* μCT scans of the explanted bone revealed small remnants of the implant within the intramedullary cavity as well as in the caudal and cranial cortical bones of the femur, even 24 weeks post-operative. As a result, the disintegration of Mg10Gd pins in smaller particles cause adverse reactions in normal bone healing and bone remodeling. Our results are contradictory to these of a study performed by Kraus et al. (6), where the ZX50, a fast degradable material, was completely degraded within 24 weeks. The fast degradation performance of ZX50 resulted in a massive callus formation and high gas release within a short time period which could cause bone damage. However, the bone was able to remodel and be healed completely within the study period of 24 weeks (6). These results are contradictory to our results of Mg10Gd, which revealed the fastest degradation behavior between the investigated materials, because a) there was no complete resolution of Mg10Gd implant remnants, and as a result, the terminology of ''disintegration'' was used to explain its degradation behavior, and b) no restitutio ad integrum of the femoral bone could be possible within the 24 weeks.

After the observed disintegration of the Mg10Gd pins into smaller particles at 12 weeks after the implantation, no further degradation could be seen at 24 and 36 weeks post-operative. No indications of further degradation, such as gas release or reduction of the degradation products amount, were observed for the high surface of remaining particles of the Mg10Gd, although, it is known that higher surface areas lead to higher degradation rates (79). Possible explanations could be: (a) the bone formation that can be observed around the particles in the high resolution μCT scans and histological staining, enclose the remnants and might decrease their further dissolution capacity. This could be inconsistency with a study performed by Kraus et al., in which a lower degradation potency of WZ21 was noticed in the cortical bone compared to the one in the medullary cavity (6). (b) Moreover, cell types such as macrophages cannot phagocyte particles larger

than 10 μm (80). Thus, the too large Mg10Gd remnant particles probably cannot be removed and degraded. (c) An additional study performed by Galli et al. have shown high degradation rate, at 4 weeks post-operative, of screw-shaped Mg10Gd implants when they are implanted in tibia rat bones and have also observed that the corrosion products of this alloy could be kept in their original shape (81). (d) Another possible explanation would be that these corrosion products may form low-dissolvable remnants that display a much slower degradation behavior.

5.2.1 Degradation performance of pure Mg, Mg2Ag and Mg10Gd in *in vitro* and *in vivo* conditions

In collaboration with Nezha Ahmad Agha (Institute of Materials Research, Division of Metallic Biomaterials, HZG, Germany) a comparison study of the degradation rates of pure Mg, Mg2Ag and Mg10Gd pin materials in *in vitro* and *in vivo* conditions at different time points was performed (3). This study was very valuable as the degradation velocities of different Mg biodegradable alloys tend to vary between the various *in vitro* set-ups as well as between the *in vitro* and *in vivo* environmental conditions. There are studies performed to search for the appropriate *in vitro* environment which could mimic the real *in vivo* situation. Unfortunately, till today, there is still missing the most suitable *in vitro* set-up.

The *in vitro* degradation rate can be determined by two different ways: a) the weight loss method (15, 48, 82-84) and b) the gas evolution method (14, 48, 75, 83). Additionally, the *in vitro* degradation rates can be calculated as an average degradation rate (8, 15) or degradation rate at different time points (33, 85).

Degradation rates of pure Mg, Mg2Ag and Mg10Gd in *in vitro* experimental set-ups have been performed in a 3 days' immersion test using Minimum Essential Medium (α-MEM) + 15 % Fetal Bovine Serum (FBS) (35) and in a 10 days' immersion test using Dulbecco's Minimum Essential Medium (DMEM)+10 % FBS

(86). Additionally, *in vitro* corrosion rates of these materials have been studied in a 5 days' immersion test focusing on sterile and unsterile DMEM (87).

In a recent review, Martinez Sanchez et al. (11) deduced that the degradation behavior of the same materials differs between *in vitro* and *in vivo* conditions and more specifically, the *in vitro* degradation rate can be higher than the *in vivo*. Also in a study performed by Myrissa et al. (3), the comparison between *in vitro* and *in vivo* results of pure Mg, Mg2Ag and Mg10Gd demonstrated that the *in vitro* degradation rates have the tendency to be higher than the *in vivo*.

Many studies have shown that the material degradation can be affected when it is incorporated in the body (11, 83, 88-91). The *in vivo* conditions of a living organism cannot be mimicked with the simplified *in vitro* experimental set-ups (82). Factors like ion concentration, blood flow, pH variations because of the degradation products, pH of body fluids, V/S ratio, the presence of proteins and the influence of cells in the surrounding tissues, can affect the degradation rate (49, 82, 92). In *in vitro* studies various cell culture media were used in order to approach the real *in vivo* conditions (12, 39, 82, 84). In our study, we used DMEM cell culture medium supplemented with 10% FBS as immersion media in order to simulate a more realistic corrosion environment by including proteins and ions. Blood plasma and DMEM solution contents differ in terms of the chloride and especially the bicarbonate ion concentration. This can affect the degradation performance of the Mg alloys due to enhancing formation of the $MgCO_3$ as the main degradation product (93, 94). In the *in vivo* study, the constant blood flow can be assumed as a non-static system which differs from our semi-static *in vitro* experimental system. In *in vivo* situation, the pH changes during the degradation procedure, is regulated by the blood buffer system. On the contrary, in the *in vitro* situation, the pH can be controlled and adjusted. Moreover, the ratio of volume solution to the surface area of the sample (V/S) is an important factor which can also affect the degradation rate of the materials (82). As a result, the choice of this ratio in *in vitro* immersion tests has to be done as close as possible to the specific *in vivo* implantation model, in studies where the *in vitro* degradation is compared to *in vivo* degradation rate (82). Proteins' interaction and adherence of different cell types to the implant surface play also a key role in the *in vivo* degradation

performance of the materials (95, 96). This can explain to some extent the lower values of the degradation rates in *in vivo* conditions and reveal the importance of both proteins and different cell interactions close to the implant (97). Furthermore, the lack of mechanical exposure in *in vitro* conditions may cause the different degradation performances of the material accompanied by different local environments.

Taking all of these into consideration, the higher degradation rate *in vitro* could be related to the insufficient simulation of a realistic *in vivo* environment. The *in vitro* experimental set-up influences the material's degradation performance and can be tailored by reconsidering immersion parameters (e.g. V/S, media selection, mechanical stimulation, cell exposition, dynamical set-up).

5.3 Part 3: Elemental distribution of a REE-containing Mg alloy

The cell cytotoxicity of Mg10Gd has been already studied in various *in vitro* cell experiments such as in primary pre-osteoblast cells (3), in human umbilical cord perivascular cells (HUCPV) (35) and in human reaming debris-derived cells (HRD) (51). The present part of the study focused on the distribution and accumulation of Gd, a rare earth element, during the degradation of the Mg10Gd alloy.

Up to now, there is no information about the distribution of a rare earth element in different organs and in blood serum samples of animal models where degradable REE-containing alloys were implanted. As a result, studies on analyzing the distribution or accumulation pattern of REE-containing biodegradable alloys are of high relevance in order to deduct safe conclusions about these materials.

In the long-term *in vivo* study, the concentrations of Mg and Gd were determined in different organs (lungs, heart, muscles, liver, spleen, kidneys and brain) and in blood serum samples. These results exhibited that the Mg element is neither accumulating in any of the investigated organs nor in the blood serum. These results, are inconsistency with the results of a study performed by O.G. Bodelón et al., in which no significant differences in the Mg levels of five organs (liver, lung, brain, kidney and spleen) were noticed between the control and the treated animal groups at 13 months post operation (98).

Moreover, no significant difference was observed with respect to the concentration of Mg in the blood serum samples between the sham (30 ± 10 mg/L) and the Mg10Gd-treated (25 ± 9 mg/L) animal groups. These results are inconsistent with other studies in which the Mg concentrations of the blood serum samples were ranged from 19 to 24 mg/L in an animal study that Mg1Sr alloy was implanted to animals (76), 31 to 34 mg/L in an animal study where Mg–3 wt % Sn–0.5wt % Mn alloy was implanted to animals (16) and 19 to 24 mg/L in an animal study where Mg6Zn alloy was implanted to animals (99).

Regarding the Gd, the results demonstrated a significant gradual accumulation of Gd in each organ of the animals with Mg10Gd pins implanted during the time of

the study period. Spleen, liver and lung showed the highest whereas brain and muscles the lowest concentration of Gd. The observed Gd distribution pattern is consistent with other studies, in which the chemical forms, as well as the administration routes of Gd, differed (100, 101). For example, a study performed by H. Liu et al. displayed high Gd accumulation especially in spleen, liver, lung, and kidneys when Gd-oxide nanotubes were administrated intraperitoneally in mice (100).

The blood serum samples exhibited Gd concentration lower than 1 µg/L and did not rise during the whole study. However, the Gd concentrations of the serum samples of both animal groups (sham and Mg10Gd-treated) are quite high, compared to the results of a study performed by Rodushkin et al., in which the Gd element in uncontaminated human and animal blood serum samples were between 1.1 and 1.8 ng/L (102). Maybe a contamination during sample collection could give a possible explanation for the “high” Gd concentrations.

The gradual accumulation of Gd element in the organs of the Mg10Gd-treated animal group is possibly because of the fast disintegration of the Mg10Gd alloy. Spleen, liver, kidneys and lungs are the organs in which the high Gd accumulation can be exhibited. These results show that Gd cannot be metabolized or excreted from the body. A study performed by Di Tie et al., 2016, have displayed that Sr^{2+} concentration is reduced in spleen, liver, and kidney organs and in blood serum samples during the degradation of Mg1Sr material within an animal study of 16 weeks (76). The authors of this study concluded that the animals could metabolize the Sr^{2+} and recover during the study period. Sr^{2+} belongs to earth alkali metal and has half of the atomic weight of Gd. Possibly, the metabolism pathway of Sr^{2+} differ to the one of a heavy rare earth element.

In literature, only few studies are available and they differ in their chemical forms and administration ways used and, as a result, varying metabolism pathways of Gd could be displayed. For example, aerosols of gadopentate dimeglumine were administrated to rats and showed a half-life of the Gd element about 2 h in the lung. This could be explained by a limited release of Gd from the chemical complex because of its stability in the lung (103, 104). On the contrary, insoluble forms of GdCl3 were administrated intratracheally to rats. These forms

metabolized very slowly and their half-life in the lung was about 136 days (54, 105).

6 CONCLUSION – OUTLOOK…..

Biodegradable Mg alloys have shown very promising results for their usage as orthopaedic medical applications. In this thesis, new insights of studying the Mg bioresorbable materials in *in vivo* conditions could be shown.

6.1 Histology in Technovit 9100 New

Technovit 9100 New embedding method has a great advantage of maintaining the interface between the implant and the tissue on molecular studies. As a consequence, the histological results of the bone tissue can be closer compared to the real *in vivo* conditions. Nevertheless, there is a requirement of testing Technovit 9100 New efficiency on different markers, in order to adapt to the standard protocol and obtain the best quality of the stainings.

6.2 Degradation performance of the alloys

Degradation performance of the binary Mg alloys, Mg2Ag and Mg10Gd, was compared to the pure Mg in a long-term study. The influence of the two alloying elements on the Mg is obvious. The alloying element Ag slows down the degradation rate of the alloy, whereas the Gd element accelerates the degradation rate of the alloy, compared to pure Mg. The Mg2Ag alloy degrades slowly and more homogeneously and shows no adverse reactions on bone healing and remodeling processes. On the contrary, Mg10Gd alloy disintegrates into small particles within 12 weeks post-operatively. The Mg10Gd ion release may cause disturbances in bone healing process and consequently, the bone is not able to recover within the study period of 36 weeks.

6.3 Elemental distribution

The elemental distribution of Mg and Gd show accumulation of the Gd ion in the animal organs of the Mg10Gd-treated animal group. The main concern of these results is that Gd could be accumulated in the rat organs even if the degradation behavior of this material was more homogeneous. Up to now, it is not clear if this accumulation leads to any long-term effects in mammals or if other REE behave in a similar pattern as Gd. For this reason, future studies should be performed, before REE-containing implants can be safely applied in humans.

Bioresorbable Mg alloys could be widely used as orthopaedic devices in bone fractures of adults and children. For this reason, their biocompatibility and safety are of great importance.

Taking all the findings of this thesis under consideration, it can be conducted that the studies have to be focused more on how the resorbable Mg alloys affect the bone healing on a cellular level, in parallel, with studies performed with μCT. Furthermore, more studies should be performed to reveal the systemic effects of the Mg alloys as well as the biocompatibility of the alloying elements.

REFERENCES

1.http://biodidac.bio.uottawa.ca/thumbnails/filedet.htm/File_name/ratt016b/File_type/gif.

2. Myrissa A, Martinelli E, Szakács G, Berger L, Eichler J, Fischerauer SF, Kleinhans C, Hort N, Schäfer U, Weinberg AM. In vivo degradation of binary Magnesium alloys - a long term study. BioNanoMaterials. 2016. doi:10.1515/bnm-2016-0006

3. Myrissa A, Agha NA, Lu Y, Martinelli E, Eichler J, Szakacs G, Kleinhans C, Willumeit-Römer R, Schäfer U, Weinberg AM. In vitro and in vivo comparison of binary Mg alloys and pure Mg. Materials Science & Engineering C. 2016;61:865–874.

4. Castellani C, Lindtner RA, Hausbrandt P, Tschegg E, Stanzl-Tschegg SE, Zanoni G, Beck S, Weinberg AM. Bone-implant interface strength and osseointegration: Biodegradable magnesium alloy versus standard titanium control. Acta Biomaterialia. 2011;7(1):432-440.

5. Brar HS, Platt MO, Sarntinoranont M, Martin PI, Manuel MV. Magnesium as a Biodegradable and Bioabsorbable Material for Medical Implants. Journal of the Minerals, Metals and Materials. 2009;61(9):31-34.

6. Kraus T, Fischerauer SF, Hänzi AC, Uggowitzer PJ, Löffler JF, Weinberg AM. Magnesium alloys for temporary implants in osteosynthesis: In vivo studies of their degradation and interaction with bone. Acta Biomaterialia. 2012;8:1230–1238.

7. Fischerauer SF, Kraus T, Wu X, Tangl S, Sorantin E, Hanzi AC, Löffler JF, Uggowitzer PJ, Weinberg AM. In vivo degradation performance of micro-arc-oxidized magnesium implants: a micro-CT study in rats. Acta Biomaterialia. 2013;9(2):5411-5420.

8. Tie D, Feyerabend F, Müller WD, Schade R, Liefeith K, Kainer KU, Willumeit R. Antibacterial biodegradable Mg-Ag alloys. European Cells & Materials. 2013;25:284-298

9. Witte F. The history of biodegradable magnesium implants: a review. Acta Biomaterialia. 2010;6(5):1680-1692.

10. Witte F, Hort N, Vogt C, Cohen S, Kainer KU, Willumeit R, Feyerabend F. Degradable Biomaterials based on Magnesium Corrosion. Current Opinion in Solid State and Materials Science. 2008;12(5-6):63-72.

11. Martinez Sanchez AH, Luthringer BJC, Feyerabend F, Willumeit R. Mg and Mg alloys: how comparable are in vitro and in vivo corrosion rates? A review. Acta Biomaterialia. 2015;13:16-31.

12. Hofstetter J, Martinelli E, Weinberg AM, Becker M, Mingler B, Uggowitzer PJ, Löffler JF. Assessing the degradation performance of ultrahigh-purity magnesium in vitro and in vivo. Corrosion Science. 2015;91:29-36.

13. Pichler K, Fischerauer S, Ferlic P, Martinelli E, Brezinsek H-P, Uggowitzer PJ, Löffler JF, Weinebrg AM. Immunological Response to Biodegradable Magnesium Implants. Journal of the Minerals, Metals and Materials. 2014;66(4):573-579.

14. Gu X, Zheng Y, Cheng Y, Zhong S, Xi T. In vitro corrosion and biocompatibility of binary magnesium alloys. Biomaterials. 2009;30(4):484-498.

15. Gu XN, Xie XH, Li N, Zheng YF, Qin L. In vitro and in vivo studies on a Mg-Sr binary alloy system developed as a new kind of biodegradable metal. Acta Biomaterialia. 2012;8(6):2360-2374.

16. Hou L, Li Z, Pan Y, Du L, Li X, Zheng Y, Li L. In vitro and in vivo studies on biodegradable magnesium alloy. Progress in Natural Science: Materials International. 2014;24(5):466-471.

17. Yang L, Huang Y, Feyerabend F, Willumeit R, Mendis C, Kainer KU, Hort N. Microstructure, mechanical and corrosion properties of Mg-Dy-Gd-Zr alloys for medical applications. Acta Biomaterialia. 2013;9(10):8499-8508.

18. Dharam PS, McGoron A. Biodegradable Magnesium Alloys: A Review of Material Development and Applications. Journal of Biomimetics, Biomaterials and Tissue Engineering. 2012;3(12):25-39.

19. Angrisani N, Seitz J-M, Meyer-Lindenberg A, Reifenrath J. Rare Earth Metals as Alloying Components in Magnesium Implants for Orthopaedic Applications. 2012.

20. Chen D, He Y, Tao H, Zhang Y, Jiang Y, Zhang X, Zhang S. Biocompatibility of magnesium-zinc alloy in biodegradable orthopedic implants. International Journal of Molecular Medicine. 2011;28(3):343-348.

21. Jähn K, Saito H, Taipaleenmäki H, Gasser A, Hort N, Feyerabend F, Schlüter H,. Rueger JM, Lehmann W, Willumeit-Römer R, Hesse E. Intramedullary Mg2Ag nails augment callus formation during fracture healing in mice. Acta Biomaterialia. 2016;36:350-360.

22. Iglesias C, Bodelón OG, Montoya R, Clemente C, Garcia-Alonso MC, Rubio JC, Escudero ML. Fracture bone healing and biodegradation of AZ31 implant in rats. Biomedical Materials. 2015;10(2).

23. Willbold E, Kalla K, Bartsch I, Bobe K, Brauneis M, Remennik S, Shechtman D, Nellesen J, Tillmann W, Vogt C, Witte F. Biocompatibility of rapidly solidified magnesium alloy RS66 as a temporary biodegradable metal. Acta Biomaterialia. 2013;9:8509-8517.

24. Ullmann B, Reifenrath J, Dziuba D, Seitz JM, Bormann D, Meyer-Lindenberg A. In Vivo Degradation Behavior of the Magnesium Alloy LANd442 in Rabbit Tibiae. Materials. 2011;4:2197-2218.

25. Willbold E, Kaya AA, Kaya RA, Beckmann F, Witte F. Corrosion of magnesium alloy AZ31 screws is dependent on the implantation site. Materials Science and Engineering B. 2011;176(20):1835-1840.

26. Rössig C, Angrisani N, Helmecke P, Besdo S, Seitz JM, Welke B, Fedchenko N, Kock H, Reifenrath J. In vivo evaluation of a magnesium-based degradable intramedullary nailing system in a sheep model. Acta Biomaterialia. 2015;25:369-383.

27. Willbold E, Witte F. Histology and research at the hard tissue–implant interface using Technovit 9100 New embedding technique. Acta Biomaterialia. 2010; 6 4447–4455.

28. Bondarenko A, Angrisani N, Meyer-Lindenberg A, Seitz JM, Waizy H, Reifenrath J. Magnesium-based bone implants: Immunohistochemical analysis of peri-implant osteogenesis by evaluation of osteopontin and osteocalcin expression. Journal of Biomedical Materials Research Part A. 2014;102(5):1449-1457.

29. Willbold E. Reebmann M, Jeffries R, Witte F. Electrochemical removal of metallic implants from Technovit 9100 New embedded hard and soft tissues prior to histological sectioning. Histochemistry and Cell Biology. 2013;140(5):585-953.

30. Yang R, Davies CM, Archer CW, Richards RG. Immunohistochemistry of matrix markers in Technovit 9100 New®-embedded undecalcified bone sections. European Cells and Materials. 2003;6:57-71.

31. Agarwal S, Curtin J, Duffy B, Jaiswal S. Biodegradable Magnesium Alloys for Orthopaedic Applications: A Review on Corrosion, Biocompatibility and Surface Modifications. Materials Science & Engineering C. 2016.

32. Chou DT, Hong D, Saha P, Ferrero J, Lee B, Tan Z, Dong Z, Kumta PN. In vitro and in vivo corrosion, cytocompatibility and mechanical properties of biodegradable Mg-Y-Ca-Zr alloys as implant materials. Acta Biomaterialia. 2013;9(10):8518-8533.

33. Hong D, Saha P, Chou DT, Lee B, Collins BE, Tan Z, Dong Z, Kumta PN. In vitro degradation and cytotoxicity response of Mg–4% Zn–0.5% Zr (ZK40) alloy as a potential biodegradable material. Acta Biomaterialia 2013;9:8534–8547.

34. Feyerabend F, Fischer J, Holtz J, Witte F, Willumeit R, Drucker H, Vogt C, Hort N. Evaluation of short-term effects of rare earth and other elements used in magnesium alloys on primary cells and cell lines. Acta Biomaterialia. 2010;6(5):1834-1842.

35. Cecchinato F, Agha NA, Martinez-Sanchez AH, Luthringer BJC, Feyerabend F, Jimbo R, Willumeit-Römer R, Wennerberg A. Influence of Magnesium Alloy Degradation on Undifferentiated Human Cells. Plos One. 2015;10(11).

36. Ge S, Wang Y, Tian J, Lei D, Yu Q, Wang G. An in vitro study on the biocompatibility of WE magnesium alloys. Journal of biomedical materials research Part B, Applied Biomaterials. 2015;104:482-487.

37. Gill P, Munroe N, Dua R, Ramaswamy S. Corrosion and Biocompatibility Assessment of Magnesium Alloys. Journal of Biomaterials and Nanobiotechnology. 2012;3:10-13.

38. Grillo CA, Alvarez F, Fernández Lorenzo de Mele MA. Cellular response to rare earth mixtures (La and Gd) as components of degradable Mg alloys for medical applications. Colloids and surfaces B, Biointerfaces. 2014;117:312-321.

39. Gu XN, Li N, Zheng YF, Ruan L. In vitro degradation performance and biological response of a Mg–Zn–Zr alloy. Materials Science and Engineering B. 2011;176(20):1778-1784.

40. Krause A, von der Höh N, Bormann D, Krause C, Bach FW, Windhagen H, Meyer-Lindenberg A. Degradation behaviour and mechanical properties of magnesium implants in rabbit tibiae. Journal of materials science Materials in Medicine. 2010;45:624-632.

41. Dziuba D, Meyer-Lindenberg A, Seitz JM, Waizy H, Angrisani N, Reifenrath J. Long-term in vivo degradation behaviour and biocompatibility of the magnesium alloy ZEK100 for use as a biodegradable bone implant. Acta Biomaterialia. 2013;9(10):8548-8560.

42. Willbold E, Gu X, Albert D, Kalla K, Bobe K, Brauneis M, Janning C, Nellesen J, Czayka W, Tillmann W, Zheng Y, Witte F. Effect of the addition of low rare earth elements (lanthanum, neodymium, cerium) on the biodegradation and biocompatibility of magnesium. Acta Biomaterialia. 2015;11:554-562.

43. Witte F, Ulrich H, Rudert M, Willbold E. Biodegradable magnesium scaffolds: Part 1: appropriate inflammatory response. Journal of Biomedical Materials Research Part A. 2007;81(3):748-756.

44. Yuen CK, Ip WY. Theoretical risk assessment of magnesium alloys as degradable biomedical implants. Acta Biomaterialia. 2010;6(5):1808-1812.

45. Wittenburg G, Volkel C, Mai R, Lauer G. Immunohistochemical comparison of differentiation markers on paraffin and plastic embedded human bone samples. Journal of Physiology and Pharmacology. 2009;60:43-49.

46. Pichler K, Musumeci G, Vielgut I, Martinelli E, Sadoghi P, Loreto C, Weinberg AM. Towards a better understanding of bone bridge formation in the growth plate - an immunohistochemical approach. Connective Tissue Research. 2013. doi: 10.3109/03008207.2013.828715.

47. Kubásek J, Vojtěch D. Structural and corrosion characterization of biodegradable Mg–RE (RE=Gd, Y, Nd) alloys. Transactions of Nonferrous Metals Society of China. 2013;23(5):1215-1225.

48. Hort N, Huang Y, Fechner D, Stormer M, Blawert C, Witte F, Vogt C, Drucker H, Willumeit R, Kainer KU, Feyerabend F. Magnesium alloys as implant materials--principles of property design for Mg-RE alloys. Acta Biomaterialia. 2010;6(5):1714-1725.

49. Poinern JGE, Brundavanam S, Fawcett D. Biomedical Magnesium Alloys: A Review of Material Properties, Surface Modifications and Potential as a Biodegradable Orthopaedic Implant. American Journal of Biomedical Engineering. 2013;2(6):218-240.

50. Gu XN, Zheng YF. A review on magnesium alloys as biodegradable materials. Frontiers of Materials Science in China. 2010;4(2):111-115.

51. Charyeva O, Dakischew O, Sommer U, Heiss C, Schnettler R, Lips KS. Biocompatibility of magnesium implants in primary human reaming debris-derived cells stem cells in vitro. Journal of Orthopaedic Traumatology. 2015;17(1):63-73.

52. Martinelli E. Intramedullary application of novel bioresorbable implants in the growing rat for osteosynthesis. Medical University Graz. 2015.

53. Kubasek J, Vojtech D. Structural characteristics and corrosion behavior of biodegradable Mg-Zn, Mg-Zn-Gd alloys. Journal of Materials Science Materials in Medicine. 2013;24(7):1615-1626.

54. Adding LC, Bannenberg GL, Gustafsson LE.. Basic Experimental Studies and Clinical Aspects of Gadolinium Salts and Chelates. Cardiovascular Drug Reviews. 2001;19(1):41-56.

55. Pagano G, Aliberti F, Guida M, Oral R, Siciliano A, Trifuoggi M, Tommasi F. Rare earth elements in human and animal health: State of art and research priorities. Environmental Research. 2015;142:215-220.

56. Drynda A, Deinet N, Braun N, Peuster M. Rare earth metals used in biodegradable magnesium-based stents do not interfere with proliferation of smooth muscle cells but do induce the upregulation of inflammatory genes. Journal of Biomedical Materials Research Part A. 2009;91A(2):360-369.

57. Shellock FG, Kanal E. Safety of Magnetic Resonance Imaging Contrast Agents. Journal of Magnetic Resonance Imaging. 1999;10:477-484.

58. Ersoy H, Rybicki FJ. Biochemical Safety Profiles of Gadolinium-Based Extracellular Contrast Agents and Nephrogenic Systemic Fibrosis. Journal of Magnetic Resonance Imaging. 2007;26:1190-1197.

59. Pedersen M. Safety Update on the Possible Causal Relationship Between Gadolinium-Containing MRI Agents and Nephrogenic Systemic Fibrosis. Journal of Magnetic Resonance Imaging. 2007;25:881-883.

60. Bernstein EJ, Schmidt-Lauber C, Kay J. Nephrogenic systemic fibrosis: a systemic fibrosing disease resulting from gadolinium exposure. Best Practice and Research Clinical Rheumatology. 2012;26(4):489-503.

61. Ramalho J, Semelka RC, Ramalho M, Nunes RH, AlObaidy M, Castillo M, Gadolinium-Based Contrast Agent Accumulation and Toxicity: An Update. American Journal of NeuroRadiology. 2015. doi:10.3174/ajnr.A4615.

62. Zobel BB, Quattrocchi CC, Errante Y, Grasso RF. Gadolinium-based contrast agents: did we miss something in the last 25 years? La radiologia medica. 2015;121(6):478-481.

63. Darrah TH, Prutsman-Pfeiffer JJ, Poreda RJ, Campbell ME, Hauschkac PV, Hannigand RE. Incorporation of excess gadolinium into human bone from medical contrast agents. Metallomics. 2009;1:479-488.

64. Fretellier N, Salhi M, Schroeder J, Siegmund H, Chevalier T, Bruneval P, Jestin-Mayer G, Delaloge F, Factor C, Mayer JM, Fabicki C, Robic B, Bonnemain JM, Idée C, Corot. Distribution profile of gadolinium in gadolinium chelate-treated renally-impaired rats: Role of pharmaceutical formulation. European Journal of Pharmaceutical Sciences. 2015;72:46-56.

65. Kanda T, Oba H, Toyoda K, Kitajima K, Furui S. Brain gadolinium deposition after administration of gadolinium-based contrast agents. Japanese Journal of Radiology. 2016;34:3-9.

66. Zhang J, Li Y, Hao X, Zhang Q, Yang K, Li L, Ma L, Wang S, Li X. Recent Progress in Therapeutic and Diagnostic Applications of Lanthanides. Mini-Reviews in Medicinal Chemistry. 2011;11(8):678-694.

67. Kostova I. Momekov G, Stancheva P. New Samarium(III), Gadolinium(III), and Dysprosium(III) Complexes of Coumarin-3-Carboxylic Acid as Antiproliferative Agents. Metal-Based Drugs. 2007. doi:10.1155/2007/15925.

68. Galvão I, Santos RG, Neves MJ. Evaluation of Gadolinium as Anticancer Agent for Brain Tumors. XL Annual Meeting of Brazilian Biochemistry and Molecular Biology Society. Brazil. 2011.

69. Magda D, Lepp C, Gerasimchuk N, Lee I, Sessler JL, Lin A, Biaglow JE, Miller RA. Redox Cycling by Motexafin Gadolinium enhances cellular response to ionizing Radiation by forming Reactive Oxygen Species. International Journal of Radiation Oncology, Biology Physics. 2001;51(4):1025-1036.

70. Magda D, Miller RA. Motexafin gadolinium: A novel redox active drug for cancer therapy. Seminars in Cancer Biology. 2006;16:466-476.

71. Thomas SR, Khuntia D. Motexafin gadolinium injection for the treatment of brain metastases in patients with non-small cell lung cancer. International Journal of Nanomedicine. 2007;2(1):79-87.

72. Thomas SR, Khuntia D. Motexafin gadolinium: a promising radiation sensitizer in brain metastasis. Expert Opinion on Drug Discovery. 2011;6(2):195-203.

73. Meyers CA. Smith JA, Bezjak A, Mehta MP, Liebmann J, Illidge T, Kunkler I, Caudrelier JM, Eisenberg PD, Meerwaldt J, Siemers R, Carrie C, Gaspar L E, Curran W, Phan SC, Miller RA, Renschler M F. Neurocognitive Function and Progression in Patients With Brain Metastases Treated With Whole-Brain Radiation and Motexafin Gadolinium: Results of a Randomized Phase III Trial. Journal of Clinical Oncology. 2004;22(1):157-165.

74. Carson FL. Histotechnology. 2nd edition, Chicago. ASCP Press. 2007.

75. Hofstetter J, Becker M, Martinelli E, Weinberg AM, Mingler B, Kilian H, Pogatscher S, Uggowitzer PJ, Löffler JF. High-Strength Low-Alloy (HSLA) Mg–Zn–Ca Alloys with Excellent Biodegradation Performance. Journal of the Minerals, Metals and Materials. 2014;66(4):566-572.

76. Tie D, Guan R, Liu H, Cipriano A, Liu Y, Wang Q, Huang Y, Hort N. An in vivo study on the metabolism and osteogenic activity of bioabsorbable Mg-1Sr alloy. Acta Biomaterialia. 2016;29:455-467.

77. Hofstetter J, Martinelli E, Pogatscher S, Schmutz P, Povoden-Karadeniz E, Weinberg AM, Uggowitzer PJ, Löffler JF. Influence of trace impurities on the in vitro and in vivo degradation of biodegradable Mg–5Zn–0.3Ca alloys. Acta Biomaterialia. 2015;23:347-353.

78. Coy AE, Viejo F, Skeldon P, Thompson GE. Susceptibility of rare-earth-magnesium alloys to micro-galvanic corrosion. Corrosion Science. 2010;52:3896-3906.

79. Johnston S, Shi Z, Dargusch MS, Atrens A. Influence of surface condition on the corrosion of ultra-high-purity Mg alloy wire. Corrosion Science. 2016;108:66-75.

80. Hallab NJ, Jacobs JJ. Biologic Effects of Implant Debris. Bulletin of the NYU Hospital for Joint Diseases. 2009;67(2):182-188.

81. Galli S, Hammel JU, Herzen J, Szakács G, Lukáč F, Vlček M, Marco I, Wennerberg A, Willumeit-Römer R, Jimbo R. Corrosion behaviour of 3 Mg-alloys in bone: a high-resolution investigation. European Cells and Materials. 2015;30:93.

82. Zhen Z, Xi TF, Zheng YF. A review on in vitro corrosion performance test of biodegradable metallic materials. Transactions of Nonferrous Metals Society of China. 2013;23(8):2283-2293.

83. Zainal Abidin NI, Rolfe B, Owen H, Malisano J, Martin D, Hofstetter J, Uggowitzer PJ, Atrens A. The in vivo and in vitro corrosion of high-purity

magnesium and magnesium alloys WZ21 and AZ91. Corrosion Science. 2013;75:354-366.

84. Gao JC, Wu S, Qiao LY, Wang Y. Corrosion behavior of Mg and Mg-Zn alloys in simulated body fluid. Transactions of Nonferrous Metals Society of China. 2008;18:588-592.

85. Huan ZG, Leeflang MA, Zhou J, Fratila-Apachitei LE, Duszczyk J. In vitro degradation behavior and cytocompatibility of Mg-Zn-Zr alloys. Journal of Materials Science: Materials in Medicine. 2010;21(9):2623-2635.

86. Charyeva O, Feyerabend F, Willumeit R, Zukowski D, Gasqueres C, Szakacs G, Agha NA, Hort N, Gensch F, Cecchinato F, Jimbo R, Wennerberg A, Lips KS. In Vitro Resorption of Magnesium Materials and its Effect on Surface and Surrounding Environment. MedCrave Online Journal of Toxicology. 2015;1(1).

87. Marco I, Feyerabend F, Willumeit-Römer R, Van der Biest O. Degradation testing of Mg alloys in Dulbecco's modified eagle medium: Influence of medium sterilization. Materials Science and Engineering C. 2016;62:68-78.

88. Witte F, Fischer J, Nellesen J, Crostack HA, Kaese V, Pisch A, Beckmann F. Windhagen H. In vitro and in vivo corrosion measurements of magnesium alloys. Biomaterials. 2006;27(7):1013-1018.

89. Walker J, Shadanbaz S, Kirkland NT, Stace E, Woodfield T, Staiger MP, Dias GJ. Magnesium alloys: predicting in vivo corrosion with in vitro immersion testing. Journal of Biomedical Materials Research Part B, Applied Biomaterials. 2012;100(4):1134-1141.

90. Xue D, Yun Y, Tan Z, Dong Z, Schulz MJ. In Vivo and In Vitro Degradation Behavior of Magnesium Alloys as Biomaterials. Journal of Material Science Technology. 2012;28(3):261–267.

91. Shadanbaz S, Walker J, Woodfield TB, Staiger MP, Dias GJ. Monetite and brushite coated magnesium: in vivo and in vitro models for degradation analysis. Journal of Materials: Science Materials in Medicine. 2013;25(1):173-183.

92. Müller WD, Nascimento ML, Zeddiese M, Córsicoc M, Gassac LM, Fernández Lorenzo de Melec MA. Magnesium and its Alloys as Degradable Biomaterials. Corrosion Studies Using Potentiodynamic and EIS Electrochemical Techniques. Materials Research. 2007;10(1):1-10.

93. Willumeit R, Fischer J, Feyerabend F, Hort N, Bismayer U, Heidrich S, Mihailova B. Chemical surface alteration of biodegradable magnesium exposed to corrosion media. Acta Biomaterialia. 2011;7:2704–2715.

94. Agha NA, Feyerabend F, Mihailova B, Heidrich S, Willumeit R. Magnesium corrosion under physiological conditions. European Cells and Materials. 2014;28:22.

95. Yang L, Hort N, Willumeit R, Feyerabend F. Effects of corrosion environment and proteins on magnesium corrosion. Corrosion Engineering, Science and Technology. 2012;47(5):335-339.

96. Eliaz N. Degradation of Implant Materials. Springer Science and Business Media, New York. 2012.

97. Willumeit-Römer R, Wendel HP, Mihailova B, Agha NA, Feyerabend F. How does blood contact change Magnesium degradation? European Cells and Materials. 2014;28:29.

98. Bodelón OG, Iglesias C, Garrido J, Clemente C, Garcia-Alonso MC, Escudero ML. Analysis of metallic traces from biodegradation of endomedullary AZ31 alloy temporary implants in rat organs after long implantation times. Biomedical Materials. 2015;10(4). doi: 10.1088/1748-6041/10/4/045015.

99. Chen Y, Yan J, Zhao C, Zhang S, Yu S, Wang Z, Wang X, Zhang X, Zheng Q. In vitro and in vivo assessment of the biocompatibility of an Mg–6Zn alloy in the bile. Journal of Materials Science: Materials in Medicine. 2014;25(2):471-480.

100. Liu H, Jia G, Chen S, Ma H, Zhao Y, Wang J, Zhang C, Wang S, Zhang J. In vivo biodistribution and toxicity of Gd2O3: Eu3+ nanotubes in mice after intraperitoneal injection. RSC Advances. 2015;5:73601-73611.

101. Nakamura Y, Tsumura Y, Tonogai Y, Shibata T, Ito Y. Differences in behavior among the chlorides of seven rare earth elements administered intravenously to rats. Fundamental and Applied Toxicology. 1997;37:106-116.

102. Rodushkin I, Ödman F, Olofsson R, Axelsson MD. Determination of 60 elements in whole blood by sector field inductively coupled plasma mass spectrometry. Journal of Analytical Atomic Spectrometry. 2000;15:937-944.

103. Berthezëne Y, Mühler A, Lang P, Shames DM, Clëment O, Rosenau W, Kuwatsuru R, Brasch RC. Safety aspects and pharmacokinetics of inhaled aerosolized gadolinium. Journal of Magnetic Resonance Imaging. 1993;3(1):125-130.

104. Hirano S, Suzuki KT. Exposure, Metabolism, and Toxicity of Rare Earths and Related Compounds. Environmental Health Perspectives. 1996;104:85-95.

105. Yoneda S, Emi N, Fujita Y, Ohmichi M, Hirano S, Suzuki KT. Effects of Gadolinium Chloride on the Rat Lung Following Intratracheal Instillation. Fundamental and Applied Toxicology. 1995;28(1):65-70.